An efficient numerical method for time domain electromagnetic wave propagation in co-axial cables

Akram Beni-Hamad, Geoffrey Beck, Sébastien Imperiale, Patrick Joly

To cite this version:

Akram Beni-Hamad, Geoffrey Beck, Sébastien Imperiale, Patrick Joly. An efficient numerical method for time domain electromagnetic wave propagation in co-axial cables. Computational Methods in Applied Mathematics, 2022, 10.1515/cmam-2021-0195 . hal-03408400v2

HAL Id: hal-03408400
https://hal.science/hal-03408400v2

Submitted on 30 Mar 2022

Akram Beni Hamad, Geoffrey Beck, Sébastien Imperiale , and Patrick Joly*

An efficient numerical method for time domain electromagnetic wave propagation in co-axial cables

Abstract: In this work we construct an efficient numerical method to solve 3D Maxwell's equations in coaxial cables. Our strategy is based upon an hybrid explicit-implicit time discretization combined with edge elements on prisms and numerical quadrature. One of the objective is to validate numerically generalized Telegrapher's models that are used to simplify the 3D Maxwell equations into a 1D problem. This is the object of the second part of the article.

Keywords: Coaxial cables, Maxwell's equations, Hybrid numerical method, Edge elements, Telegrapher's models, Numerical simulation.

1 Introduction and motivation

The numerical simulation in the time domain of electromagnetic wave propagation in coaxial cables networks is an important issue in many industrial applications, whether it concerns communications network or power supply of devices. Indeed, one of the issue is the non-destructive testing of these cables. Non-destructive testing of defects [3], [1], [5] often relies on forward modelling and simulations of the electric quantities propagating in the cables. The underlying models that are mainly used are based on representation of the coaxial cables has 1D model called telegrapher model which deals on the propagation of the voltage and the current along infinitesimal RLCG quadripole (see [24] for cylindrical case) although the real propagation of electromagnetic waves is governed by 3D Maxwell's equations.

More in detail, a straight cable of length L is made of a dielectric material that surrounds a metallic inner-wire (whose presence is needed for allowing for wave propagation along the cable at frequencies of interest) and is surrounded by an outer sheath. The inner and outer structures are both made of perfect conducting materials so that the electromagnetic field is confined in the dielectric part (for questions about non-perfectly conducting inner and outer wires, readers can refer to [7]). This dielectric part can be defined as a longitudinal succession of plane transverse 2D plane cross-sections with one hole. More precisely, x_3 denoting the abscissa along the cable, the domain of propagation Ω for the electric field is

$$\Omega = \bigcup_{x_3 \in \,[-\frac{L}{2},\frac{L}{2}\,]} S(x_3) \tag{1}$$

where the cross section $S(x_3)$ is the difference between two connected open sets of $\mathbb{R}^2$

$$S(x_3) = \mathcal{O}_e(x_3) \setminus \overline{\mathcal{O}_i(x_3)}, \quad \mathcal{O}_e(x_3), \mathcal{O}_i(x_3) \subset \mathbb{R}^2 \text{ connected}, \quad \overline{\mathcal{O}_i(x_3)} \subset \mathcal{O}_i(x_3), \tag{2}$$

Akram Beni Hamad, POEMS (UMR CNRS-INRIA-ENSTA Paris)Institut Polytechnique de Paris, France/ LAMMDA-ESST Hammam Sousse, Universié de Sousse, Tunisie, e-mail: akram.beni-hamad@ensta-paris.fr

Geoffrey Beck, Departement de mathématiques et applications, ´ Ecole normale supérieure, CNRS, ´ PSL University,Paris, France, e-mail: geoffrey.beck.poems@gmail.com

Sébastien Imperiale , M3DISIM (Inria, LMS, Ecole Polytechnique, CNRS), Institut Polytechnique de Paris, France, e-mail: sebastien.imperiale@inria.fr

***Corresponding author: Patrick Joly,** POEMS (UMR CNRS-INRIA-ENSTA Paris) Institut Polytechnique de Paris, France, e-mail: patrick.joly@inria.fr

which means that the boundary of $S(x_3)$ has two connected component:

$$\partial S(x_3) = \Gamma_e(x_3) \cup \Gamma_i(x_3) \tag{3}$$

where $\Gamma_e(x_3) := \partial\mathcal{O}_e(x_3)$ (resp. $\Gamma_i(x_3) := \partial\mathcal{O}_i(x_3)$) will be called the exterior boundary (resp. the interior boundary) of $S(x_3)$.

In industrial applications, cables are thin, mathematically we will consider that its transverse dimension is proportional to a small parameter $\delta \ll 1$. By using an asymptotic analysis of the 3D Maxwell equations with $\delta \to 0$, several 1D simplified models of such kind were rigorously derived in [4]. If some of this models have been justified from a mathematical point of view by error estimates when the cable has cylindrical geometry, to our knowledge, there is no existing quantitative numerical comparison between 1D model and 3D Maxwell's theory. Doing so requires performing 3D simulations with 3D Maxwell's equations. This is a computational challenge particularly since the cable is thin and the goal of this paper is to precisely addressed these issues. To better outline the difficulties to handle, it is worth while mentioning that a typical simulation problem contains naturally three length :

- the diameter of the cable δ,
- the mean wavelength along the cable λ,
- the characteristic length of the propagation L.

Due to the elongated structure of the propagation domain Ω, it is natural to use elongated meshes with step size h in the longitudinal direction x_3 and step size h_T in the transverse directions. These parameters are constrained by the characteristics of the problems as follows

- $h_T \ll \delta$, for well dealing with the internal structure of the cable and well representing the variations of the electromagnetic field inside each cross section,
- $h \ll \lambda$, to represent accurately the variations of the solution in the longitudinal direction.

In practice, as $\delta \ll L$, we will have $h_T \ll h$ which leads to a huge number of degrees of freedom.

When time discretization, with time step Δt, is involved, one has traditionally to face a choice:

(i) Either one uses a fully explicit time discretization in which case, for stability reasons (CFL conditions), Δt is constrained by the small space step h_T, i. e. $\Delta t \le c^{-1}\, h_T$ where c is a constant that has the dimension of a velocity. This clearly imposes very small time steps.
(ii) Either one uses a fully implicit and unconditionally stable time discretization. In this case, there is no more constrain on Δt for stability reasons but the problem is that a large linear system has to be solved at each time iteration.

In summary, each of the two above solutions would lead to prohibitive computational costs (if not out of reach computations): either the number of time steps is much too large, case (i), either the cost of each time iteration is much too high, case (ii). That is why our objective to find a trade off between solutions (i) and (ii) in which

(a) Δt would be constrained by the longitudinal space step h only, as for a 1D propagation problem discretized with an explicit scheme
(b) The cost of each time iteration would remain reasonable.

This objective will be attained through an hybrid time discretization approach that would be implicit in the transverse directions, ensuring (a), but explicit in the longitudinal direction, ensuring (b).

The outline of this article is the following:

- Section 2 is dedicated to the full discretization in space and time of the Maxwell's equation in straight coaxial cables. In a first section we derive a specific form of the Maxwell's equation, Section 2.1, where we make explicit the equations satisfy by the transverse and longitudinal component of the electric field. Section 2.2 is dedicated to the semi-discretization in space. We first treat the discretization with respect to the longitudinal variable (Section 2.2.1) then with respect to the transverse variable (Section 2.2.2). it turns out that the proposed discretization can be re-interpreted via prismatic edge's element [8, 11] on prisms (Section 2.2.4). Finally, in Section 2.2 we describe the semi-discrete scheme in an algebraic form. Section 2.3 concerns the time discretization . In Section 2.3.1, we propose an hybrid implicit-explicit scheme, whose complexity and stability properties are analyzed Section 2.3.2 and 2.3.3.
- In the sections 3 and 4 we use our scheme in order to validate numerically the generalized 1D Telegrapher model of [16], that is recap Section 3.1. We describe in Section 3.2, the method used for the discretization of this 1D model , which involve non-local in time operators. The last section, Section 4, is dedicated to the validation tests.

2 A numerical method for cylindrical cables

We consider a cylindrical cable for which the cross section is independent of x_3 (see Figure 1) and we assume, for simplicity of the exposition, that the length L is infinite so that

$$\Omega = S \times \mathbb{R}, \quad (\text{ i.e. } S(x_3) = S \ \text{(independent of } x_3), \quad \partial S = \Gamma_e \cup \Gamma_i. \tag{4}$$

The dielectric material is characterized by the electrical permittivity ε and the magnetic permeability μ

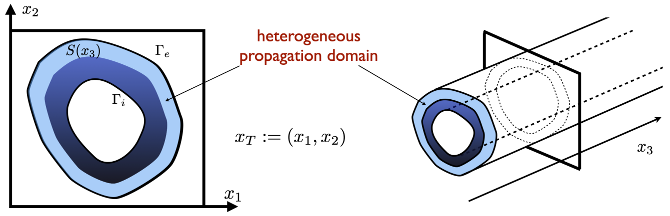

Fig. 1: Left : slice of the domain, right :the geometry of the domain Ω.

which are both function of the space variable $\mathbf{x} \in \Omega$ that satisfy the usual assumptions

$$0 < \mu_- \leq \mu(\mathbf{x}) \leq \mu_+, \quad 0 < \varepsilon_- \leq \varepsilon(\mathbf{x}) \leq \varepsilon_+ \quad \text{a.e.}\, \mathbf{x} = (x_1, x_2, x_3) \in \Omega.$$

We shall also consider the possibility that the cable can be, at least locally, conducting, wich is modelled through the conductivity σ,

$$0 \leq \sigma(\mathbf{x}) \leq \sigma_+, \quad \text{a.e. } \mathbf{x} = (x_1, x_2, x_3) \in \Omega. \tag{5}$$

Note that the translational invariance in x_3 concerns only the geometry of the domain Ω, not the coefficients ε , σ and μ. The propagation of waves in the cable Ω, through the unknowns $\mathbf{E}(\mathbf{x}, \mathbf{t})$ (the electric field) and $\mathbf{H}(\mathbf{x}, \mathbf{t})$ (the magnetic field) is governed by 3D Maxwell's equations completed with perfectly conducting boundary conditions on $\partial\Omega$,

$$\left\{ \begin{array}{ll} \varepsilon\, \partial_t \mathbf{E} + \sigma\, \mathbf{E} - \boldsymbol{\nabla} \times \mathbf{H} = \mathbf{0}, & \text{in } \ \Omega \times \mathbb{R}^+. \\[1ex] \mu\, \partial_t \mathbf{H} + \boldsymbol{\nabla} \times \mathbf{E} = \mathbf{0}, & \text{in } \ \Omega \times \mathbb{R}^+, \\[1ex] \mathbf{E} \times \mathbf{n} = 0, & \text{on } \ \partial\Omega \times \mathbb{R}^+, \end{array} \right. \tag{6}$$

where t is the time, $\boldsymbol{\nabla}\times$ the 3D curl operator and $\mathbf{n}$ stands for the unit outward normal. The model is completed with initial conditions (for simplicity again we have suppose the absence of source terms, without any loss of generality)

$$\mathbf{E}(\cdot,0)=\mathbf{E}_0,\quad \mathbf{H}(\cdot,0)=\mathbf{H}_0. \tag{7}$$

Our method will be developed for the second order electric field formulation of the problem, obtained after elimination of the magnetic field,

$$\left|\begin{array}{ll} \varepsilon\,\partial_t^2\mathbf{E}+\sigma\,\partial_t\mathbf{E}-\boldsymbol{\nabla}\times\,\mu^{-1}\,\boldsymbol{\nabla}\times\mathbf{E}=\mathbf{0}, & \text{in } \Omega\times\mathbb{R}^+,\\[2ex] \mathbf{E}\times\mathbf{n}=\mathbf{0}, & \text{on } \partial\Omega\times\mathbb{R}^+,\\[2ex] \mathbf{E}(\cdot,0)=\mathbf{E}_0,\quad \partial_t\mathbf{E}(\cdot,0)=\varepsilon^{-1}\big(\boldsymbol{\nabla}\times\mathbf{H}_0-\sigma\,\mathbf{E}_0\big) & \text{in } \Omega. \end{array}\right. \tag{8}$$

Our approach will be based on a particular rewriting of that well separates the roles of the longitudinal and transverse space variables (resp, longitudinal and transverse electric fields).

For the simplicity, without any loss generality, we shall present our method in the case $\sigma=0$. The conductivity will be reintroduced in Section 3.

2.1 An adequate reformulation of the continuous problem

We introduce the longitudinal and transverse space variables

$$\mathbf{x}=(\mathbf{x}_T,x_3),\quad \mathbf{x}_T=(x_1,x_2)$$

and decompose the electric field into transverse ($\mathbf{E}_T$) and longitudinal (E_3) components,

$$\mathbf{E}=\begin{pmatrix}\mathbf{E}_T\\[1ex] E_3\end{pmatrix}\qquad\text{with}\quad \mathbf{E}_T=\begin{pmatrix}E_1\\[1ex] E_2\end{pmatrix}.$$

To rewrite (8), we shall use the following transverse curl and gradient operators (note that the index T refers to transverse derivatives),

$$\mathrm{rot}_T\mathbf{E}_T=\partial_1E_2-\partial_2E_1,\quad \mathbf{rot}_T\,E_3=\begin{pmatrix}\partial_2E_3\\[1ex] -\partial_1E_3\end{pmatrix},\quad \nabla_T\,E_3=\begin{pmatrix}\partial_1E_3\\[1ex] \partial_2E_3\end{pmatrix}. \tag{9}$$

The first one is a scalar rotational operator whereas the second is a vectorial rotational operator which can be seen as a "rotated" gradient

$$\mathbf{rot}_T\,E_3=-\mathbf{e}_3\times\nabla_TE_3,\quad\text{with}\quad \mathbf{e}_3\times E_T=\begin{pmatrix}-E_2\\[1ex] E_1\end{pmatrix}\qquad\text{and}\qquad \mathbf{e}_3=(0,0,1)^t.$$

These rotational operators are related to the 3D curl operator via

$$\boldsymbol{\nabla}\times\mathbf{E}=\begin{pmatrix}\mathbf{rot}_TE_3+\mathbf{e}_3\times\partial_3\mathbf{E}_T\\[1ex] \mathrm{rot}_T\mathbf{E}_T\end{pmatrix}.$$

Thus, the Maxwell's equations (8) rewrite (this is straightforward computations)

$$\left|\begin{array}{l} \varepsilon\,\partial_t^2\mathbf{E}_T-\partial_3\big(\mu^{-1}\partial_3\mathbf{E}_T\big)+\mathbf{rot}_T\big(\mu^{-1}\mathrm{rot}_T\mathbf{E}_T\big)+\partial_3\big(\mu^{-1}\nabla_TE_3\big)=0,\\[2ex] \varepsilon\,\partial_t^2E_3+\mathrm{rot}_T\big(\mu^{-1}\mathbf{rot}_TE_3\big)+\mathrm{div}_T\big(\mu^{-1}\partial_3\mathbf{E}_T\big)=0. \end{array}\right. \tag{10}$$

2.2 Space discretization

We shall use a Galerkin approach based of the weak (variational) formulation of (10). In order to give the weak formulation of this problem, we introduce the following functional spaces

$$\left|\begin{array}{l} H(\mathbf{rot};\Omega) := \big\{\big(\mathbf{E}_T, E_3\big) \in L^2(\Omega)^2 \times L^2(\Omega)\,/\,\mathbf{rot}_T E_3 \,+\, \mathbf{e}_3 \times \partial_3 \mathbf{E}_T \in L^2(\Omega)^2, \mathrm{rot}_T \mathbf{E}_T \in L^2(\Omega)\big\}, \\[2mm] V := H_0(\mathbf{rot};\Omega) = \big\{\mathbf{E} \in H(\mathbf{rot};\Omega)\,/\,\mathbf{E}\times\mathbf{n} = 0 \text{ on } \partial\Omega\big\}. \end{array}\right.$$

We aim at finding $\big(\mathbf{E}_T, E_3\big) \in V$ such that for any test function $\big(\widetilde{\mathbf{E}}_T, \widetilde{E}_3\big) \in V$, we have

$$\left|\begin{array}{l} \dfrac{d^2}{dt^2}\,\mathbf{m}\big(\mathbf{E}_T, \widetilde{\mathbf{E}}_T\big) + \mathbf{k}_3\big(\mathbf{E}_T, \widetilde{\mathbf{E}}_T\big) + \mathbf{k}_T\big(\mathbf{E}_T, \widetilde{\mathbf{E}}_T\big) - c_{3T}\big(E_3, \widetilde{\mathbf{E}}_T\big) = 0, \\[2mm] \dfrac{d^2}{dt^2}\,m\big(E_3, \widetilde{E}_3\big) + k_T\big(E_3, \widetilde{E}_3\big) - c_{3T}\big(\widetilde{E}_3, \mathbf{E}_T\big) = 0, \end{array}\right. \tag{11}$$

with the continuous bilinear forms

$$\left\{\begin{array}{ll} \mathbf{m}\big(\mathbf{E}_T, \widetilde{\mathbf{E}}_T\big) := \displaystyle\int_\Omega \varepsilon\, \mathbf{E}_T \cdot \widetilde{\mathbf{E}}_T, & m\big(E_3, \widetilde{E}_3\big) := \displaystyle\int_\Omega \varepsilon\, E_3\, \widetilde{E}_3, \\ \mathbf{k}_T\big(\mathbf{E}_T, \widetilde{\mathbf{E}}_T\big) := \displaystyle\int_\Omega \mu^{-1}\, \mathrm{rot}_T \mathbf{E}_T\; \mathrm{rot}_T \widetilde{\mathbf{E}}_T, & k_T\big(E_3, \widetilde{E}_3\big) := \displaystyle\int_\Omega \mu^{-1}\, \nabla_T E_3\; \nabla_T \widetilde{E}_3, \\ \mathbf{k}_3\big(\mathbf{E}_T, \widetilde{\mathbf{E}}_T\big) := \displaystyle\int_\Omega \mu^{-1}\, \partial_3 \mathbf{E}_T \cdot \partial_3 \widetilde{\mathbf{E}}_T, & c_{3T}\big(E_3, \mathbf{E}_T\big) = \displaystyle\int_\Omega \mu^{-1}\, \nabla_T E_3 \cdot \partial_3 \mathbf{E}_T. \end{array}\right. \tag{12}$$

The stiffness bilinear forms $\mathbf{k}_T, k_T$ and $\mathbf{k}_3$ do not couple transverse and longitudinal fields. We use bold letters when they apply to transverse fields. The index T means that only transverse derivatives are involved while the index 3 means that only x_3-derivatives are involved. Oppositely the bilinear form c_{3T} couple the transverse and longitudinal fields and mixes the x_3 and transverse derivatives. We shall call it the coupling bilinear form. Note that, at the exception of c_{3T}, these bilinear forms are symmetric and positive. The coupling term can easily be controlled thanks to Cauchy-Schwarz inequality

$$|c_{3T}\big(E_3, \mathbf{E}_T\big)| \leq k_T\big(E_3, E_3\big)^{\frac{1}{2}}\; \mathbf{k}_3\big(\mathbf{E}_T, \mathbf{E}_T\big)^{\frac{1}{2}}. \tag{13}$$

We now deal with the space discretization. For the presentation, we find useful to treat successively the discretization in x_3 first (Section 2.2.1) then in the transverse variables $\mathbf{x}_T$ (Section 2.2.2), which is by the way justified by the "cylindrical structure" of Ω. However, we can reinterpret the result of these two step as the result of direct $3D$ discretization (Section 2.2.4).

2.2.1 Semi-discretization in x_3.

For the longitudinal discretization, we decomposed the cable Ω into small cylindrical cells

$$\mathcal{C}_{j+\frac{1}{2}} = \{(\mathbf{x}_T, x_3) \in \Omega \;/\; jh \leq x_3 \leq (j+1)h\}, \quad j \in \mathbb{Z} \tag{14}$$

These cells of size h in the x_3 direction (h is the longitudinal space step) are separated by transverse cross section $S_j, j \in \mathbb{Z}$ (see Figure 2) where, by definition

$$\forall\, \nu \in \mathbb{R}, \quad \mathcal{S}_\nu = \{(\mathbf{x}_T, \nu h), \mathbf{x}_T \in S\}. \tag{15}$$

We know describe $\mathbf{V}_h$ the approximation space of the 3D space $H(\mathbf{rot};\Omega)$, it is the product space

$$\mathbf{V}_h := \mathbf{V}_{h,T} \times V_{h,\ell} \subset H(\mathbf{rot};\Omega), \tag{16}$$

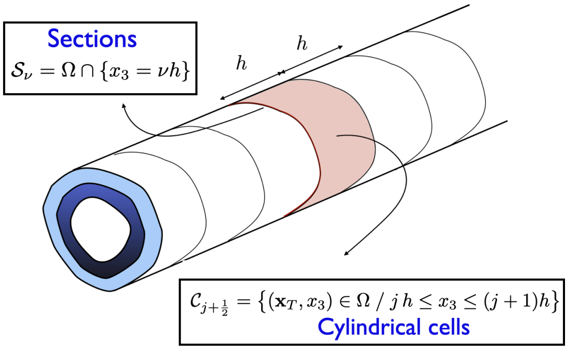

Fig. 2: Schematic of the sections and the cells of the cable.

where the approximation of transverse field $\mathbf{E}_T$ lives in $\mathbf{V}_{h,T}$ whereas the approximation of the longitudinal variable E_3 lives in $V_{h,\ell}$. On the one hand, $\mathbf{V}_{h,T}$ is made of $\mathbb{P}_1$ continuous function in three directions with value in the 2D $H(\mathrm{rot}_T, S)$ space

$$\mathbf{V}_{h,T} := \Big\{\mathbf{E}_{T,h} \in C^0\big(\mathbb{R}; H(\mathrm{rot}_T, S)\big) \,/\, \forall\, j,\ \mathbf{E}_T|_{\mathcal{C}_{j+\frac{1}{2}}} \in \mathbb{P}_1\big(\mathbb{R}; H(\mathrm{rot}_T, S)\big)\Big\}, \tag{17}$$

where, $H(\mathrm{rot}_T; S) := \big\{\mathbf{E}_T \in L^2(\Omega)^2 \times L^2(\Omega) \,/\, \mathrm{rot}_T \mathbf{E}_T \in L^2(\Omega)\big\}$.

In other words, for any $\mathbf{E}_T \in \mathbf{V}_{h,T}$, denoting $\mathbf{E}_{T,j} = \mathbf{E}_T|_{S_j} \in H(\mathrm{rot}_T, S)$, we have

$$\mathbf{E}_T(\mathbf{x}_T, x_3) = \sum_{j \in \mathbb{Z}} \mathbf{E}_{T,j}(\mathbf{x}_T)\, w_j(x_3), \tag{18}$$

where w_j is the usual hat function associated with $x_3 = jh$ (see Figure 3).

On the other hand, the space $V_{h,\ell}$ is made of piecewise constant ($\mathbb{P}_0$) functions in x_3 with values in $H^1(S)$

$$V_{h,\ell} := \{E_3 : \Omega \to \mathbb{R} \,/\, \forall\, j,\ E_3|_{\mathcal{C}_{j+\frac{1}{2}}} \in \mathbb{P}_0\big(\mathbb{R}; H^1(S)\big)\big\}. \tag{19}$$

In other words, for any $E_3 \in V_{h,\ell}$, there exists $E_{3,j+\frac{1}{2}} \in H^1(S), j \in \mathbb{Z}$ such that

$$E_3(\mathbf{x}_T, x_3) = \sum_{j \in \mathbb{Z}} E_{3,j+\frac{1}{2}}(\mathbf{x}_T)\, \chi_{j+\frac{1}{2}}(x_3), \quad E_{3,j+\frac{1}{2}} = E_3|_{S_{j+\frac{1}{2}}} \tag{20}$$

where $\chi_{j+\frac{1}{2}}$ is the characteristic function of the interval $(jh, (j+1)h]$ (see Figure 3).

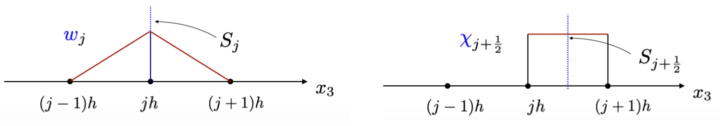

Fig. 3: The 1D basis functions w_j (left) and $\chi_{j+\frac{1}{2}}$ (right)

The semi-discrete problem is obtained essentially by rewriting the variational formulation (11) after replacing the continuous space by the semi-discrete space $\mathbf{V}_h$. More precisely, this problem reads:

Find $\big(\mathbf{E}_{T,h}, E_{3,h}\big) \in \mathbf{V}_h := \mathbf{V}_{h,T} \times V_{h,\ell}$ such that for any $\big(\widetilde{\mathbf{E}}_{T,h}, \widetilde{E}_{3,h}\big) \in \mathbf{V}_h$,

$$\left|\begin{aligned} &\frac{d^2}{dt^2}\,\mathbf{m}_h\big(\mathbf{E}_{T,h}, \widetilde{\mathbf{E}}_{T,h}\big) + \mathbf{k}_3\big(\mathbf{E}_{T,h}, \widetilde{\mathbf{E}}_{T,h}\big) + \mathbf{k}_{T,h}\big(\mathbf{E}_{T,h}, \widetilde{\mathbf{E}}_{T,h}\big) - c_{3T}\big(E_{3,h}, \widetilde{\mathbf{E}}_{T,h}\big) = 0, \\ &\frac{d^2}{dt^2}\, m\big(E_{3,h}, \widetilde{E}_{3,h}\big) + k_T\big(E_{3,h}, \widetilde{E}_{3,h}\big) - c_{3T}\big(\widetilde{E}_{3,h}, \mathbf{E}_{T,h}\big) = 0. \end{aligned}\right. \tag{21}$$

Apart from the functional spaces, there is another difference between (11) and (21) which makes our approximation non-conforming in the finite element sense. This ingredient is in fact very important for the efficiency of the method and to end up with numerical schemes which will be explicit in x_3. More precisely, we approximate the two bilinear forms that involve transverse fields and do not involve x_3-derivatives, namely $\big(\mathbf{m}$ and $\mathbf{k}_T\big)$, by using a quadrature formula in the x_3 direction, transforming them into $\big(\mathbf{m}_h$ and $\mathbf{k}_{T,h}\big)$. More precisely, with respect to the definition (12) of the exact bilinear forms

$$\big(\mathbf{m}, \mathbf{k}_T\big) \quad \longrightarrow \quad \big(\mathbf{m}_h, \mathbf{k}_{T,h}\big) \quad \text{via} \quad \int\limits_{\Omega} \varepsilon\, f \to \oint\limits_{\Omega} \varepsilon\, f, \quad \int\limits_{\Omega} \mu^{-1} f \to \oint\limits_{\Omega} \mu^{-1} f, \tag{22}$$

where $\oint_\Omega \varepsilon\, f$ (resp. $\oint_\Omega \mu^{-1} f$) refers to a nodal quadrature formula in x_3, well adapted to the measure $\varepsilon\, d\mathbf{x}$ (resp. $\mu^{-1}\, d\mathbf{x}$). More precisely, for $f \in C^0\big(\mathbb{R}; L^1(S)\big) \cap L^1\big(\Omega\big)$, we set

$$\oint\limits_{\Omega} \varepsilon\, f = h \sum_j \int\limits_S \varepsilon_{j+\frac12} \Big(\frac{f_{j+1} + f_j}{2}\Big)\, d\mathbf{x}_T, \quad f_j = f|_{S_j} \tag{23}$$

where $\varepsilon_{j+\frac12}(\mathbf{x}_T)$ holds for the 1D mean value of ε in $C_{j+\frac12}$,

$$\text{a.e. } \mathbf{x}_T \in S, \quad \varepsilon_{j+\frac12}(\mathbf{x}_T) = \frac{1}{h} \int\limits_{jh}^{(j+1)h} \varepsilon(\mathbf{x}_T, x_3)\, dx_3, \tag{24}$$

Remark 2.1. *One has the Fubini-like formula*

$$\oint\limits_{\Omega} \varepsilon\, f = \int\limits_S \Big(\oint\limits_{\mathbb{R}} \varepsilon(\mathbf{x_T}, x_3)\; f(\mathbf{x_T}, x_3)\; dx_3 \Big) d\mathbf{x}_T \tag{25}$$

with the 1D quadrature formula, for any $g \in L^1(\mathbb{R}) \cap C^0(\mathbb{R})$*,*

$$\oint\limits_{\mathbb{R}} \varepsilon(\mathbf{x_T}, x_3)\; g(x_3)\; dx_3 := h \sum_j \varepsilon_{j+\frac12}(\mathbf{x_T}) \big(\tfrac{g((j+1)h) + g(jh)}{2}\big). \tag{26}$$

Note that this formula can also be written

$$\oint\limits_{\mathbb{R}} \varepsilon(\mathbf{x_T}, x_3)\; g(x_3)\; dx_3 := \int\limits_{\mathbb{R}} \varepsilon_h(\mathbf{x_T}, x_3)\; \pi_{1,h} g(x_3)\; dx_3. \tag{27}$$

where ε_h *is the piecewise constant approximation of* ε *with its mean value inside each interval* $(jh, (j+1)h]$ *and* $\pi_{1,h} g$ *is the* $\mathbb{P}_1$*-interpolate of* g*.*

One has the fundamental property (1D mass lumping) about hat functions

$$\forall\, \ell \neq j, \quad \oint\limits_{\mathbb{R}} \varepsilon(\mathbf{x_T}, x_3)\, w_j(x_3)\, w_\ell(x_3)\, dx_3 := 0 \tag{28}$$

For what follows, it will be useful to have an expanded version of the bilinear forms appearing in (21), when acting on the semi-discrete spaces. Since functions in $V_{h,\ell}$ are piecewise constant, the bilinear forms m and k_T are naturally "block diagonal". More precisely, using the decomposition (20),

$$\begin{aligned} m\big(E_{3,h}, \widetilde{E}_{3,h}\big) &= \sum_{j \in \mathbb{Z}} m_{j+\frac12}\big(E_{3,j+\frac12}, \widetilde{E}_{3,j+\frac12}\big) \equiv h \sum_{j \in \mathbb{Z}} \int\limits_{S_{j+\frac12}} \varepsilon\, E_{3,j+\frac12} \cdot \widetilde{E}_{3,j+\frac12}, \\ k_T\big(E_{3,h}, \widetilde{E}_{3,h}\big) &= \sum_{j \in \mathbb{Z}} k_{j+\frac12}\big(E_{3,j+\frac12}, \widetilde{E}_{3,j+\frac12}\big) \equiv h \sum_{j \in \mathbb{Z}} \int\limits_{S_{j+\frac12}} \mu^{-1}\, \nabla_T E_{3,j+\frac12} \cdot \nabla_T \widetilde{E}_{3,j+\frac12} \end{aligned} \tag{29}$$

In the same way, thanks to the quadrature (23), the bilinear forms $\mathbf{m}_h$ and $\mathbf{k}_{T,h}$ are block diagonal too. More precisely, using the decomposition (18),

$$\begin{aligned} \mathbf{m}_h\big(\mathbf{E}_{T,h},\widetilde{\mathbf{E}}_{T,h}\big) &= \sum_{j\in\mathbb{Z}} \mathbf{m}_{h,j}\big(\mathbf{E}_{T,j},\widetilde{\mathbf{E}}_{T,j}\big) \equiv h\sum_{j\in\mathbb{Z}}\int_{S_j} \varepsilon\,\mathbf{E}_{T,j}\cdot\widetilde{\mathbf{E}}_{T,j} \\ \mathbf{k}_{T,h}\big(\mathbf{E}_{T,h},\widetilde{\mathbf{E}}_{T,h}\big) &= \sum_{j\in\mathbb{Z}} \mathbf{k}_{h,j}\big(\mathbf{E}_{T,j},\widetilde{\mathbf{E}}_{T,j}\big) \equiv h\sum_{j\in\mathbb{Z}}\int_{S_j} \mu^{-1}\,\mathrm{rot}_T\mathbf{E}_{T,j}\cdot\mathrm{rot}_T\widetilde{\mathbf{E}}_{T,j} \end{aligned} \tag{30}$$

Finally, for the last two bilinear forms, one computes that

$$\begin{aligned} \mathbf{k}_3\big(\mathbf{E}_{T,h},\widetilde{\mathbf{E}}_{T,h}\big) &= h\sum_{j\in\mathbb{Z}}\mu^{-1}_{j+\frac12}\int_S \frac{\mathbf{E}_{T,j+1}-\mathbf{E}_{T,j}}{h}\cdot\frac{\widetilde{\mathbf{E}}_{T,j+1}-\widetilde{\mathbf{E}}_{T,j}}{h}, \\ c_{3T}\big(E_{3,h},\widetilde{\mathbf{E}}_{T,h}\big) &= h\sum_{j\in\mathbb{Z}}\mu^{-1}_{j+\frac12}\int_S \nabla_T E_{3,j+\frac12}\cdot\frac{\widetilde{\mathbf{E}}_{T,j+1}-\widetilde{\mathbf{E}}_{T,j}}{h}, \end{aligned} \tag{31}$$

where, as in (24), we have defined

$$\text{a.e. } \mathbf{x}_T\in S,\quad \mu^{-1}_{j+\frac12}(\mathbf{x}_T) = \frac{1}{h}\int_{jh}^{(j+1)h} \mu^{-1}(\mathbf{x}_T,x_3)\,dx_3, \tag{32}$$

2.2.2 Full space discretization

For the discretization in the transverse variables, we introduce a conforming triangular mesh $\mathcal{T}$ (in the usual finite element sense) of S with step-size h_T (see Figure 4), namely the transverse space step. In the sequel we shall denote N the number of nodes of this mesh and N_e the number of (interior) edges. We shall use the letter $\mathbf{h}$ to denote the set of approximation parameters in space, namely

$$\mathbf{h} := (h, h_T). \tag{33}$$

The fully discrete space, indexed with $\mathbf{h}$ takes the same form of the semi-discrete space as in (16),

$$\mathbf{V}_\mathbf{h} = \mathbf{V}_{\mathbf{h},T}\times V_{\mathbf{h},\ell}$$

The transverse field $\mathbf{E_T}$ is searched piecewise linear continuous in x_3 with value in the classical 2D Nedelec space [22],[23] denoted $\mathbf{V}_{h_T}(S)$ (with respect to (17), we simply replace $H(\mathrm{rot}_T,S)$ by $\mathbf{V}_{h_T}(S)$).

$$\mathbf{V}_{\mathbf{h},T} := \big\{\mathbf{E}_{T,h}\in C^0\big(\mathbb{R};\mathbf{V}_{h_T}(S)\big)\ /\ \forall\, j,\ \mathbf{E}_T|_{\mathcal{C}_{j+\frac12}}\in\mathbb{P}_1\big(\mathbb{R};\mathbf{V}_{h_T}(S)\big)\big\}. \tag{34}$$

$$\text{with}\quad \left\{\begin{aligned} &\mathbf{V}_{h_T}(S) := \big\{\mathbf{E}_T\in H(\mathrm{rot}_T,S)\big)\ /\ \forall\, K\in\mathcal{T}, \mathbf{E}_T|_K\in\mathcal{N}_{2D}\big\}, \\ &\mathcal{N}_{2D} := \big\{a\,(x_2,-x_1)^t+\mathbf{b}, (a,\mathbf{b})\in\mathbb{R}\times\mathbb{R}^2\big\}\subset\mathbb{P}_1^2. \end{aligned}\right. \tag{35}$$

The longitudinal field E_3 is searched piecewise constant in x_3 with value in the standard $\mathbb{P}_1$ finite element space for $H^1(S)$ (with respect to (19), we simply replace $H^1(S)$ by $V_{h_T}(S)$) :

$$\left\{\begin{aligned} &V_{\mathbf{h},\ell} := \big\{E_3:\Omega\to\mathbb{R}\ /\ \forall\, j, \forall\, x_3\in[jh,(j+1)h]\ \ E_3(\cdot,x_3) = E_{3,j+\frac12}\in V_{h_T}(S)\big\}, \\ &V_{h_T}(S) := \big\{E_3\in H^1(S)\ /\ \forall\, K\in\mathcal{T},\ E_3|_K\in\mathbb{P}_1\big\}. \end{aligned}\right. \tag{36}$$

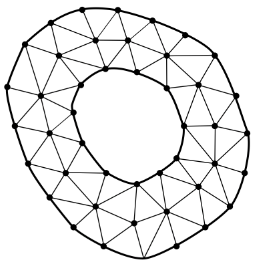

Fig. 4: Triangular mesh of S with step-size h_T

We have thus two type of degrees of freedom for the discrete electric field. The first ones, associated to the transverse field, are denoted $\mathbb{E}_{T,\mathbf{h}} \equiv \left\{ \mathbb{E}_{T,j} \right\}$, $\mathbb{E}_{T,j} \in \mathbb{R}^{N_e}$, is the vector of the tangential components of the discrete transverse electric field along the edges in the cross section S_j.

The second ones, for the longitudinal field, are denoted $\mathbb{E}_{3,\mathbf{h}} \equiv \left\{ \mathbb{E}_{3,j+\frac{1}{2}} \right\}$, where $\mathbb{E}_{3,j+\frac{1}{2}} \in \mathbb{R}^{N}$ is the vector of the values of the discrete longitudinal field at the nodes of the mesh.

Transverse field in each section S_j

Longitudinal field in each section $S_{j+\frac{1}{2}}$

Fig. 5: Two types of degrees of freedom

In the end we have the transverse field unknowns $\mathbb{E}_{T,j}$ and longitudinal fields unknowns $\mathbb{E}_{3,j+\frac{1}{2}}$ alternate from one cross section to the other (see Figure 5 and 6).

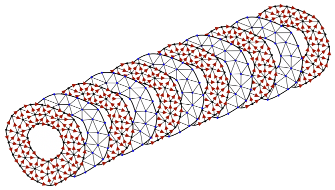

Fig. 6: Degrees of freedom in the 3D mesh.

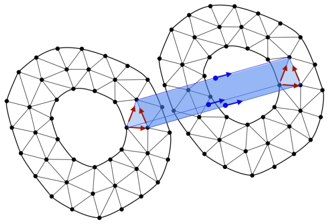

Fig. 7: Prismatic mesh.

2.2.3 Reinterpretation as prismatic edge elements

It is worthwhile reinterpreting the space as the result of a 3D finite element approximation of $H(\mathbf{rot},\Omega)$ based on a prismatic mesh $\mathcal{T}_{3D}$ of the cable Ω,

$$\mathcal{T}_{3D} := \left\{\mathcal{P}_{K,j} \;/\; K \in \mathcal{T}, j \in \mathbb{Z}\right\} \qquad \text{such that } \Omega = \bigcup_{K,j} \mathcal{P}_{K,j}, \tag{37}$$

where the prim $\mathcal{P}_{K,j}$ is defined as (note that it has only longitudinal or transverse faces, cf. Figure 7)

$$\mathcal{P}_{K,j} = K \times [jh,(j+1)h]. \tag{38}$$

The space is nothing but a space of prismatic edge elements, namely,

$$\mathbf{V_h} := \left\{\mathbf{E_h} \in H(\mathbf{rot},\Omega) \;/\; \forall\, \mathcal{P}_{K,j} \in \mathcal{T}_{3D},\ \mathbf{E_h}|_{\mathcal{P}_{K,j}} \in \mathcal{R}\right\}, \tag{39}$$

where $\mathcal{R} = \left\{\mathbf{E} = (\mathbf{E}_T, E_3) \;/\; \mathbf{E}_T(\cdot,x_3) \in \mathbb{P}_1(\mathbb{R};\mathcal{N}^{2D}),\ E_3(\cdot,x_3) \in \mathbb{P}_0(\mathbb{R};\mathbb{P}_1(\mathbb{R}^2))\right\} \subset \mathbb{P}_1^3$. Note that the use of edge elements on prisms has been already studied (see [8, 11]), in regard to these works, the originality of our approach lies in the time discretization, that will treat differently in-plane (i.e. in the plane of the sections) and out-of-plane interactions between degrees of freedom.

2.2.4 The semi-discrete scheme and its algebraic form

The fully semi-discrete variational problem reads

Find $\left(\mathbf{E}_{T,\mathbf{h}}, E_{3,\mathbf{h}}\right) \in \mathbf{V_h} := \mathbf{V}_{\mathbf{h},T} \times V_{\mathbf{h},\ell}$ such that for any $\left(\mathbf{E}_{T,\mathbf{h}}, E_{3,\mathbf{h}}\right) \in \mathbf{V_h}$,

$$\left|\begin{aligned}
&\frac{d^2}{dt^2}\,\mathbf{m}_h\big(\mathbf{E}_{T,\mathbf{h}},\widetilde{\mathbf{E}}_{T,\mathbf{h}}\big) + \mathbf{k}_3\big(\mathbf{E}_{T,\mathbf{h}},\widetilde{\mathbf{E}}_{T,\mathbf{h}}\big) + \mathbf{k}_{T,h}\big(\mathbf{E}_{T,\mathbf{h}},\widetilde{\mathbf{E}}_{T,\mathbf{h}}\big) - c_{3T}\big(E_{3,\mathbf{h}},\widetilde{\mathbf{E}}_{T,\mathbf{h}}\big) = 0,\\
&\frac{d^2}{dt^2}\,m\big(E_{3,\mathbf{h}},\widetilde{E}_{3,\mathbf{h}}\big) + k_T\big(E_{3,\mathbf{h}},\widetilde{E}_{3,\mathbf{h}}\big) - c_{3T}\big(\widetilde{E}_{3,\mathbf{h}},\mathbf{E}_{T,\mathbf{h}}\big) = 0.
\end{aligned}\right. \tag{40}$$

To write the problem in more algebraic form, we introduce here the (infinite) vector degrees of freedom namely (with obvious notation)

$$\mathbb{E}_{\mathbf{h}} = \begin{pmatrix}\mathbb{E}_{T,\mathbf{h}}\\ \mathbb{E}_{3,\mathbf{h}}\end{pmatrix} \equiv \begin{pmatrix}\mathbb{E}_{T,j}\\ \mathbb{E}_{3,j+\frac{1}{2}}\end{pmatrix} \in \mathbb{V}_{\mathbf{h}} := \mathbb{V}_{\mathbf{h},T} \times \mathbb{V}_{\mathbf{h},3} \tag{41}$$

where $\mathbb{V}_{\mathbf{h},T}$ and $\mathbb{V}_{\mathbf{h},3}$ are the Hilbert spaces

$$\mathbb{V}_{\mathbf{h},T} = \ell^2\big(\mathbb{Z},\mathbb{R}^{N_e}\big), \quad \mathbb{V}_{\mathbf{h},3} = \ell^2(\mathbb{Z},\mathbb{R}^N).$$

According to the above, it is clear that (40) has an equivalent algebraic form,

$$\mathbf{M_h}\frac{d^2\mathbb{E}_{\mathbf{h}}}{dt^2} + \mathbf{K_h}\,\mathbb{E}_{\mathbf{h}} = 0. \tag{42}$$

where $\mathbf{M_h}$ and $\mathbf{K_h}$ are the mass and stiffness matrices in $\mathbb{V}_{\mathbf{h}}$ (their obvious and classical definition is omitted here). According to the decomposition of $\mathbf{V_h}$ between transverse and longitudinal fields , the mass matrix $\mathbf{M_h}$ has the following block diagonal form

$$\mathbf{M_h} = \begin{pmatrix}\mathbf{M}_{\mathbf{h}}^T & 0\\ 0 & M_{\mathbf{h}}^3\end{pmatrix} \tag{43}$$

and, in particular, thanks to numerical quadrature, $\mathbf{M}_{\mathbf{h}}^{T}$ (resp. $\mathbf{M}_{\mathbf{h}}^{3}$) is block diagonal by sections with blocks of dimension N_e (resp. N). On the other hand, the stiffness matrix $\mathbf{K}_{\mathbf{h}}$ can be written, according (40) as

$$\mathbf{K}_{\mathbf{h}} = \begin{pmatrix} \mathbf{K}_{3,\mathbf{h}} + \mathbf{K}_{T,\mathbf{h}} & \mathbf{C}_{3T,\mathbf{h}} \\ \mathbf{C}_{3T,\mathbf{h}}^{*} & K_{T,\mathbf{h}} \end{pmatrix} \tag{44}$$

where there is also some block decomposition by sections. More precisely, the global problem can be rewritten "section by section" separating the roles of the transverse and longitudinal fields as follows

$$\left|\begin{aligned} & \mathbb{M}_j \frac{d^2\mathbb{E}_{T,j}}{dt^2} + \mathbb{K}_{T,j}\,\mathbb{E}_{T,j} - \frac{1}{h}\left(\mathbb{M}_{j+\frac{1}{2}}\,\frac{\mathbb{E}_{T,j+1}-\mathbb{E}_{T,j}}{h} - \mathbb{M}_{j-\frac{1}{2}}\,\frac{\mathbb{E}_{T,j}-\mathbb{E}_{T,j-1}}{h}\right) \\ & \qquad\qquad\qquad\qquad + \frac{\mathbb{C}_{3T,j+\frac{1}{2}}\,\mathbb{E}_{3,j+\frac{1}{2}} - \mathbb{C}_{3T,j-\frac{1}{2}}\mathbb{E}_{3,j-\frac{1}{2}}}{h} = 0, \\ & \mathrm{M}_{j+\frac{1}{2}}\frac{d^2\mathbb{E}_{3,j+\frac{1}{2}}}{dt^2} + \mathrm{K}_{T,j+\frac{1}{2}}\,\mathbb{E}_{3,j+\frac{1}{2}} - \mathbb{C}^{*}_{3T,j+\frac{1}{2}}\,\frac{\mathbb{E}_{T,j+1}-\mathbb{E}_{T,j}}{h} = 0, \end{aligned}\right. \tag{45}$$

which well emphasizes how the various "interface unknowns" are coupled or decoupled. Note that

- The matrices $\mathbb{M}_j$, $\mathbb{M}_{j+\frac{1}{2}}$ and $\mathbb{K}_{T,j}$ are of dimension $N_e \times N_e$: $\mathbb{M}_j$ (resp. $\mathbb{M}_{j+\frac{1}{2}}$) is a 2D (vectorial) mass matrix (which is not diagonal) corresponding to the multiplication by ε (resp. by μ^{-1}) while $\mathbb{K}_{T,j}$ is a 2D stiffness matrix corresponding to the action of the operator $\mathbf{rot}_T(\mu^{-1}\mathrm{rot}_T)$.
- The matrices $\mathrm{M}_{j+\frac{1}{2}}$ and $\mathrm{K}_{T,j+\frac{1}{2}}$ are of dimension $N \times N$: it corresponds to the multiplication by ε while $\mathrm{K}_{T,j+\frac{1}{2}}$ is a 2D stiffness matrix corresponding to the action of the operator $\mathrm{div}_T(\mu^{-1}\nabla_T)$.
- The matrices $\mathbb{C}_{3T,j+\frac{1}{2}}$ are $N \times N_e$ and corresponds to the action of the operator $\mu^{-1}\nabla_T$.
- Their transpose correspond $\mathbb{C}^{*}_{3T,j+\frac{1}{2}}$ to the action of the operator $-\mathrm{div}_T(\mu^{-1}\cdot)$.

2.3 Time discretization

Our method will be based on a tricky decomposition of the stiffness matrix $\mathbf{K}_{\mathbf{h}}$ (cf. (44))

$$\mathbf{K}_{\mathbf{h}} = \mathbf{K}_{\mathbf{h}}^{i} + \mathbf{K}_{\mathbf{h}}^{e} \quad \text{where} \quad \mathbf{K}_{\mathbf{h}}^{i} = \begin{pmatrix} \mathbf{K}_{T,\mathbf{h}} & 0 \\ 0 & K_{T,\mathbf{h}} \end{pmatrix} \quad \text{and} \quad \mathbf{K}_{\mathbf{h}}^{e} = \begin{pmatrix} \mathbf{K}_{3,\mathbf{h}} & \mathbf{C}_{3T,\mathbf{h}} \\ \mathbf{C}_{3T,\mathbf{h}}^{*} & 0 \end{pmatrix}. \tag{46}$$

The interest of the decomposition lies in the following double observation

- $\mathbf{K}_{\mathbf{h}}^{i}$ is adapted to implicit time discretization because the matrix is positive and block diagonal: for this reason it is "easy" to invert (it corresponds to a series 2D problems, see section 2.3.2).
- Oppositely $\mathbf{K}_{\mathbf{h}}^{e}$ is adapted to explicit time discretization because of the presence of the ”3” index which corresponds to the x_3 derivative: this matrix couples all the interfaces and has no sign.

2.3.1 A hybrid implicit-explicit scheme

According to (46), we rewrite (42) as

$$\mathbf{M}_{\mathbf{h}}\frac{d^2\mathbb{E}_{\mathbf{h}}}{dt^2} + \mathbf{K}_{\mathbf{h}}^{e}\,\mathbb{E}_{\mathbf{h}} + \mathbf{K}_{\mathbf{h}}^{i}\,\mathbb{E}_{\mathbf{h}} = 0$$

and propose a numerical scheme in which $\mathbb{E}_{\mathbf{h}}$ at time $t^n = n\Delta t$ is approximated differently depending on the fact that it is in factor of $\mathbf{K}_{\mathbf{h}}^{e}$ or $\mathbf{K}_{\mathbf{h}}^{i}$. More precisely, and according to what we said in the introduction of this section, we propose the following hybrid implicit-explicit leap frog scheme, in which $\theta \in [0,1]$ is a parameter,

$$\mathbf{M}_{\mathbf{h}}\frac{\mathbb{E}_{\mathbf{h}}^{n+1} - 2\,\mathbb{E}_{\mathbf{h}}^{n} + \mathbb{E}_{\mathbf{h}}^{n-1}}{\Delta t^2} + \mathbf{K}_{\mathbf{h}}^{i}\,\{\mathbb{E}_{\mathbf{h}}^{n}\}_{\theta} + \mathbf{K}_{\mathbf{h}}^{e}\,\mathbb{E}_{\mathbf{h}}^{n} = 0, \tag{47}$$

where $\{\mathbb{E}^n_{\mathbf{h}}\}_\theta$ corresponds to the weighted mean value

$$\{\mathbb{E}^n_{\mathbf{h}}\}_\theta := \theta\, \mathbb{E}^{n+1}_{\mathbf{h}} + (1-2\theta)\, \mathbb{E}^n_{\mathbf{h}} + \theta\, \mathbb{E}^{n-1}_{\mathbf{h}}, \quad \theta \in [0,1]. \tag{48}$$

Clearly, this scheme is a mix between the explicit leap frog scheme and the implicit θ-scheme (or centered Newmark scheme). It is obviously second order accurate in Δt whatever is θ. How implicit is this scheme is the subject of the next section.

Remark 2.2. *The above ideas already appeared in the literature in various contexts and for different purposes. One class of works concern locally implicit time stepping is which different parts of the computational domain are treated differently : see for instance [25], [13] or more recently [13] for fourth order schemes. In [9], [2], the objective was to treat in a particular way the boundary condition arising from the formulation of elastodynamics by way of potentials introduced for treatinf separately the two types of waves. In [14], the objective was to treat explicitly the linear part of the model and implicitly the nonlinear one. Here, these are the direction of space differentiation, longitudinal or transverse, which are treated in a different manner. In some sense, except the fact that we are dealing with a strongly anisotropic problem, our work has some similarities with the ADI schemes proposed by Fornberg and Lee (see [19], [20] and [15] for an analysis).*

2.3.2 Computational complexity

According to the rewriting "section by section" (45) of the discrete problem, we can rewrite the scheme

$$\left|\begin{array}{l}
\mathbb{M}_j \dfrac{\mathbb{E}^{n+1}_{T,j} - 2\mathbb{E}^n_{T,j} + \mathbb{E}^{n-1}_{T,j}}{\Delta t^2} + \mathbb{K}_{T,j}\left(\theta\, \mathbb{E}^{n+1}_{T,j} + (1-2\theta)\, \mathbb{E}^n_{T,j} + \theta\, \mathbb{E}^{n-1}_{T,j}\right) \\[2ex]
-\dfrac{1}{h}\left(\mathbb{M}_{j+\frac12}\, \dfrac{\mathbb{E}^n_{T,j+1} - \mathbb{E}^n_{T,j}}{h} - \mathbb{M}_{j-\frac12}\, \dfrac{\mathbb{E}^n_{T,j} - \mathbb{E}^n_{T,j-1}}{h}\right) + \dfrac{\mathbb{C}_{3T,j+\frac12}\, \mathbb{E}^n_{3,j+\frac12} - \mathbb{C}_{3T,j-\frac12}\mathbb{E}^n_{3,j-\frac12}}{h} = 0, \\[3ex]
\mathrm{M}_{j+\frac12} \dfrac{\mathbb{E}^{n+1}_{3,j+\frac12} - 2\mathbb{E}^n_{3,j+\frac12} + \mathbb{E}^{n-1}_{3,j+\frac12}}{\Delta t^2} + \mathrm{K}_{T,j+\frac12}\left(\theta\, \mathbb{E}^{n+1}_{3,j+\frac12} + (1-2\theta)\, \mathbb{E}^n_{3,j+\frac12} + \theta\, \mathbb{E}^{n-1}_{3,j+\frac12}\right) \\[2ex]
\qquad\qquad\qquad\qquad\qquad\qquad\qquad - \mathbb{C}^*_{3T,j+\frac12}\, \dfrac{\mathbb{E}^n_{T,j+1} - \mathbb{E}^n_{T,j}}{h} = 0
\end{array}\right.$$

Looking at where the superscript $n+1$ appears in the above equations, one sees that at each time step one has to invert (this can be done in parallel) the matrices

$$\mathbb{M}_j + \theta\, \Delta t^2 \mathbb{K}_{T,j} \quad \text{and } \mathrm{M}_{j+\frac12} + \theta\, \Delta t^2 \mathrm{K}_{T,j+\frac12}.$$

This illustrates the fact that the scheme is implicit only in the transverse direction. This corresponds to solving numerically, using appropriate finite elements,

- a series of coercive 2D vectorial curl-curl problems of the type

$$\gamma\, \mathbf{rot}_T(\mu^{-1}\mathrm{rot}_T \mathbf{u}) + \mathbf{u} = \mathbf{g} \quad \text{in S}, \quad \gamma = \theta\, \Delta t^2\, \varepsilon^{-1} > 0,$$

- a series of coercive 2D scalar div-grad problems of the type

$$-\gamma\, \mathrm{div}_T(\mu^{-1}\nabla_T u) + u = g \quad \text{in S}, \quad \gamma = \theta\, \Delta t^2\, \varepsilon^{-1} > 0.$$

2.3.3 Stability analysis

For our main theorem, we need to introduce the function $\alpha_h(\mathbf{x}_T)$ defined by:

$$\alpha_h(\mathbf{x}_T)^2 := \sup_{u_h \in \mathbb{P}_{1,h}} \frac{\int_{\mathbb{R}} \mu(\cdot, \mathbf{x}_T)^{-1} |u_h'|^2}{\oint_{\mathbb{R}} \varepsilon(\cdot, \mathbf{x}_T) |u_h|^2}, \tag{49}$$

where

$$\mathbb{P}_{1,h} := \{u_h \in C^0(\mathbb{R}) \cap L^2(\mathbb{R}) \;/\; \forall\, j \in \mathbb{Z},\; u_h|_{[jh,(j+1)h]} \in \mathbb{P}_1\} \tag{50}$$

It is also useful to introduce the velocity of electromagnetic waves in Ω

$$\forall\, \mathbf{x} \in \Omega, \quad c(\mathbf{x}) = \varepsilon(\mathbf{x})^{-\frac{1}{2}} \mu(\mathbf{x})^{-\frac{1}{2}}, \quad c^+ := \sup_{\Omega} c(\mathbf{x}) \tag{51}$$

Theorem 2.3. The fully discrete scheme (47) is stable if $\theta > \frac{1}{4}$ and

$$\frac{\Delta t^2}{4} \, \|\alpha_h\|_\infty^2 \le \frac{4\theta - 1}{4\theta} \tag{52}$$

with α_h defined in (49). The CFL condition (52) is in particular satisfied as soon as

$$\frac{c^+ \Delta t}{h} < \sqrt{\frac{4\theta - 1}{4\theta}}. \tag{53}$$

Proof. Since there is no possible ambiguity, and for the sake of simplicity, we shall use the same notation $\big(\cdot,\cdot\big)$ for inner products in $\mathbb{V}_{\mathbf{h},T}$ and $\mathbb{V}_{\mathbf{h},3}$. Below, we refer to (41) and the dot is systematically used for the appropriate Euclidean scalar product that may change from one occurrence to the other,

$$\begin{gathered} \big(\mathbb{U}_{\mathbf{h},T}, \widetilde{\mathbb{U}}_{\mathbf{h},T}\big) := \sum_{j \in \mathbb{Z}} \mathbb{U}_{T,j} \cdot \widetilde{\mathbb{U}}_{T,j}, \quad \big(\mathbb{U}_{\mathbf{h},3}, \widetilde{\mathbb{U}}_{\mathbf{h},3}\big) := \sum_{j \in \mathbb{Z}} \mathbb{U}_{3,+\frac{1}{2}} \cdot \widetilde{\mathbb{U}}_{3,j+\frac{1}{2}} \\ \big(\mathbb{U}_{\mathbf{h}}, \widetilde{\mathbb{U}}_{\mathbf{h}}\big) = \big(\mathbb{U}_{\mathbf{h},T}, \widetilde{\mathbb{U}}_{\mathbf{h},T}\big) + \big(\mathbb{U}_{\mathbf{h},3}, \widetilde{\mathbb{U}}_{\mathbf{h},3}\big) \end{gathered} \tag{54}$$

The proof is done in three steps using an energy approach.

Step 1 : Discrete energy conservation. We use the two key (but standard) identities :

$$\mathbb{E}_{\mathbf{h}}^n = \{\mathbb{E}_{\mathbf{h}}^n\}_{\frac{1}{4}} - \tfrac{1}{4}\left(\mathbb{E}_{\mathbf{h}}^{n+1} - 2\,\mathbb{E}_{\mathbf{h}}^n + \mathbb{E}_{\mathbf{h}}^{n-1}\right), \quad \{\mathbb{E}_{\mathbf{h}}^n\}_\theta = \{\mathbb{E}_{\mathbf{h}}^n\}_{\frac{1}{4}} + \big(\theta - \tfrac{1}{4}\big)\left(\mathbb{E}_{\mathbf{h}}^{n+1} - 2\,\mathbb{E}_{\mathbf{h}}^n + \mathbb{E}_{\mathbf{h}}^{n-1}\right).$$

This allows us to rewrite our scheme as a perturbation of the $\frac{1}{4}$-scheme.

$$\mathbf{M}_h(\Delta t)\, \frac{\mathbb{E}_{\mathbf{h}}^{n+1} - 2\,\mathbb{E}_{\mathbf{h}}^n + \mathbb{E}_{\mathbf{h}}^{n-1}}{\Delta t^2} + \mathbf{K}_{\mathbf{h}}\, \{\mathbb{E}_{\mathbf{h}}^n\}_{\frac{1}{4}} = 0,$$

where we have set

$$\mathbf{M}_{\mathbf{h}}(\Delta t) = \mathbf{M}_h^i(\Delta t) - \tfrac{\Delta t^2}{4}\, \mathbf{K}_{\mathbf{h}}^e \quad \text{and} \quad \mathbf{M}_h^i(\Delta t) := \mathbf{M}_{\mathbf{h}} + \big(\theta - \tfrac{1}{4}\big)\, \Delta t^2\, \mathbf{K}_{\mathbf{h}}^i. \tag{55}$$

Taking the scalar product (in $\mathbb{V}_{\mathbf{h}} := \mathbb{V}_{\mathbf{h},T} \times \mathbb{V}_{\mathbf{h},3}$) of the above equation with $\frac{\mathbb{E}_{\mathbf{h}}^{n+1} - \mathbb{E}_{\mathbf{h}}^n}{\Delta t}$ we classically deduce, thanks to the symmetry of all matrices) the conservation of the discrete energy

$$\mathcal{E}_{\mathbf{h}}^{n+\frac{1}{2}} := \frac{1}{2}\left[\left(\mathbf{M}_{\mathbf{h}}(\Delta t) \frac{\mathbb{E}_{\mathbf{h}}^{n+1} - \mathbb{E}_{\mathbf{h}}^n}{\Delta t}, \frac{\mathbb{E}_{\mathbf{h}}^{n+1} - \mathbb{E}_{\mathbf{h}}^n}{\Delta t}\right) + \left(\mathbf{K}_{\mathbf{h}}\Big(\frac{\mathbb{E}_{\mathbf{h}}^{n+1} + \mathbb{E}_{\mathbf{h}}^n}{2}\Big), \frac{\mathbb{E}_{\mathbf{h}}^{n+1} + \mathbb{E}_{\mathbf{h}}^n}{2}\right)\right].$$

Step 2 : Derivation of the sufficient stability condition (52).

This will be simply obtained from showing the positivity of the discrete energy $\mathcal{E}_{\mathbf{h}}^{n+\frac{1}{2}}$, that amounts to the positivity of the modified mass matrix $\mathbf{M}_h(\Delta t)$. The idea is first to ensure the positivity of $\mathbf{M}_{\mathbf{h}}^i(\Delta t)$ only choosing adequately θ (typically $\theta > \frac{1}{4}$ then to control $\Delta t^2\, \mathbf{K}_{\mathbf{h}}^e$ by playing on Δt. As we are going to see this can be done by imposing to Δt a lower bound that only sees the longitudinal space step h.

To be more precise, assuming $\theta > \frac{1}{4}$, we first obtain a lower bound of the quadratic form associated with $\mathbf{M}^i_h(\Delta t)$. Recalling that

$$\mathbf{M}_{\mathbf{h}} = \begin{pmatrix} \mathbf{M}^T_{\mathbf{h}} & 0 \\ 0 & M^3_{\mathbf{h}} \end{pmatrix} \quad \text{and} \quad \mathbf{K}^i_{\mathbf{h}} = \begin{pmatrix} \mathbf{K}_{T,\mathbf{h}} & 0 \\ 0 & K_{T,\mathbf{h}} \end{pmatrix},$$

we drop, in the expression of $\mathbf{M}^i_{\mathbf{h}}(\Delta t)$, the positive blocks associated with $M^3_{\mathbf{h}}$ and $(\theta - \frac{1}{4})\mathbf{K}_{T,\mathbf{h}}$, one deduces that for any $\mathbb{U}_{\mathbf{h}} \in \mathbb{V}_{\mathbf{h}}$,

$$\big(\mathbf{M}^i_{\mathbf{h}}(\Delta t)\mathbb{U}_{\mathbf{h}}, \mathbb{U}_{\mathbf{h}}\big) \geq \big(\mathbf{M}^T_{\mathbf{h}}\,\mathbb{U}_{T,\mathbf{h}}, \mathbb{U}_{T,\mathbf{h}}\big) + \big(\theta - \tfrac{1}{4}\big)\,\Delta t^2 \big(K_{T,\mathbf{h}}\mathbb{U}_{3,\mathbf{h}}, \mathbb{U}_{3,\mathbf{h}}\big), \tag{56}$$

where we draw again the attention of the reader that, according to (54) and depending on the context, the notation $(\cdot,\cdot)$ is the scalar product in $\mathbb{V}_{\mathbf{h}}$, $\mathbb{V}_{\mathbf{h},T}$ and $\mathbb{V}_{\mathbf{h},3}$. We now obtain an upper bound for the quadratic form associated with $\mathbf{K}^e_{\mathbf{h}}$. For this, we first remark that the inequality (13) results into

$$\big(\mathbf{C}_{3T,\mathbf{h}}\mathbb{U}_{3,\mathbf{h}}, \mathbb{U}_{T,\mathbf{h}}\big) \equiv \big(\mathbb{U}_{3,\mathbf{h}}, \mathbf{C}^*_{3T,\mathbf{h}}\mathbb{U}_{T,\mathbf{h}}\big) \leq \Big(K_{T,\mathbf{h}}\mathbb{U}_{3,\mathbf{h}}, \mathbb{U}_{3,\mathbf{h}}\Big)^{\frac{1}{2}} \big(\mathbf{K}_{3,\mathbf{h}}\mathbb{U}_{\mathbf{h},T}, \mathbb{U}_{\mathbf{h},T}\big)^{\frac{1}{2}} \tag{57}$$

so that, from the block decomposition (46) of $\mathbf{K}^e_{\mathbf{h}}$, one deduces the inequality

$$\big|\big(\mathbf{K}^e_{\mathbf{h}}\mathbb{U}_{\mathbf{h}}, \mathbb{U}_{\mathbf{h}}\big)\big| \leq \big(\mathbf{K}_{3,\mathbf{h}}\mathbb{U}_{\mathbf{h},T}, \mathbb{U}_{\mathbf{h},T}\big) + 2\,\big(K_{T,\mathbf{h}}\mathbb{U}_{3,\mathbf{h}}, \mathbb{U}_{3,\mathbf{h}}\big)^{\frac{1}{2}} \big(\mathbf{K}_{3,\mathbf{h}}\mathbb{U}_{\mathbf{h},T}, \mathbb{U}_{\mathbf{h},T}\big)^{\frac{1}{2}}.$$

Finally, in order to exploit (56), we control the matrix $\mathbf{K}_{3,\mathbf{h}}$ with the help of the mass matrix $\mathbf{M}^T_{\mathbf{h}}$ that appears in the lower bound (56). This is where the longitudinal space step h will appear via the function α_h.More precisely, let $\mathbf{U}_{h,T} \in \mathbf{V}_{h,T}$ associated to the vector $\mathbb{U}_{\mathbf{h},T} \in \mathbb{V}_{\mathbf{h},T}$, by definition of $\mathbf{K}_{3,\mathbf{h}}$

$$\big(\mathbf{K}_{3,\mathbf{h}}\mathbb{U}_{\mathbf{h},T}, \mathbb{U}_{\mathbf{h},T}\big) = \mathbf{k}_3(\mathbf{U}_{h,T}, \mathbf{U}_{h,T}) = \int_\Omega \mu^{-1}|\partial_3 \mathbf{U}_{h,T}|^2.$$

Using the Fubini's theorem and $\mathbf{U}_{h,T} = (\mathbf{U}_{h,1}, \mathbf{U}_{h,2})$, we get

$$\Big(\mathbf{K}_{3,\mathbf{h}}\mathbb{U}_{\mathbf{h},T}, \mathbb{U}_{\mathbf{h},T}\Big) = \int_S \Big(\int_{\mathbb{R}} \mu^{-1}(\mathbf{x}_T, x_3)\big(|\partial_3 \mathbf{U}_{h,1}(\mathbf{x}_T, x_3)|^2 + |\partial_3 \mathbf{U}_{h,2}(\mathbf{x}_T, x_3)|^2\big)\, dx_3\Big) d\mathbf{x}_T.$$

Then, by definition (49) of the function α_h, and since, for fixed $\mathbf{x}_T$, each function $\mathbf{U}_{h,1}(\mathbf{x}_T,\cdot)$ and $\mathbf{U}_{h,1}(\mathbf{x}_T,\cdot)$ belongs to $\mathbb{P}_{1,h}$ by definition (17) of $\mathbf{V}_{h,T}$, we have

$$\big(\mathbf{K}_{3,\mathbf{h}}\mathbb{U}_{\mathbf{h},T}, \mathbb{U}_{\mathbf{h},T}\big) \leq \int_S \alpha_h(\mathbf{x}_T)\Big(\oint_{\mathbb{R}} \varepsilon(\mathbf{x}_T, x_3)\big(|\mathbf{U}_{h,1}(\mathbf{x}_T, x_3)|^2 + |\mathbf{U}_{h,2}(\mathbf{x}_T, x_3)|^2\big)\, dx_3\Big) d\mathbf{x}_T$$

so that, referring to the Fubini-like formula (25) and the definition of $\mathbf{m}_h$ (see (12, 22)), we get

$$\big(\mathbf{K}_{3,\mathbf{h}}\mathbb{U}_{\mathbf{h},T}, \mathbb{U}_{\mathbf{h},T}\big) \leq \|\alpha_h\|_\infty\, \mathbf{m}_h(\mathbf{U}_{h,T}, \mathbf{U}_{h,T}) \equiv \|\alpha_h\|_\infty\, \big(\mathbf{M}^T_{\mathbf{h}}\mathbb{U}_{\mathbf{h},T}, \mathbb{U}_{\mathbf{h},T}\big). \tag{58}$$

Finally, joining (56) and (58) to the definition (55) of $\mathbf{M}_{\mathbf{h}}(\Delta t)$, we obtain

$$\big(\mathbf{M}_{\mathbf{h}}(\Delta t)\,\mathbb{U}_{\mathbf{h}}, \mathbb{U}_{\mathbf{h}}\big) \geq q(X,Y) := \big(1 - \|\alpha_h\|^2_\infty\, \tfrac{\Delta t^2}{4}\big)\, X^2 - \|\alpha_h\|_\infty\, \tfrac{\Delta t^2}{2}\, XY + \big(\theta - \tfrac{1}{4}\big)\, \Delta t^2\, Y^2, \tag{59}$$

where we have set $X = \big(\mathbf{M}^T_{\mathbf{h}}\,\mathbb{U}_{\mathbf{h},T}, \mathbb{U}_{\mathbf{h},T}\big)^{\frac{1}{2}}$ and $Y = \big(K_{T,\mathbf{h}}\mathbb{U}_{3,\mathbf{h}}, \mathbb{U}_{3,\mathbf{h}}\big)^{\frac{1}{2}}$.

The stability condition (52) is finally obtained by writing that the quadratic $q(X,Y)$ form is positive.

Step 3 : Derivation of the sufficient stability condition (53).

With respect to (52), (53) is a (slightly) stronger but more explicit (thus more useful) sufficient stability condition. It is a direct consequence of the upper bound

$$\|\alpha_h\|^2_\infty \leq \frac{4\, c_+^2}{h^2}.$$

This estimate is a straightforward consequence of the definition of the weighted quadrature formula (26). Indeed, for any $u_h \in P_{1,h}$ and by definition of c^+

$$\int_{\mathbb{R}} \mu(\cdot, \mathbf{x}_T)^{-1} |u_h'|^2 \leq c_+^2 \int_{\mathbb{R}} \varepsilon(\cdot, \mathbf{x}_T) |u_h'|^2.$$

However, since u_h' is piecewise constant, we have, with $u_j := u_h(jh)$ and by definition (24) of $\varepsilon_{j+\frac{1}{2}}$,

$$\int_{\mathbb{R}} \mu(\cdot, \mathbf{x}_T)^{-1} |u_h'|^2 \leq c_+^2 \sum_{j \in Z} \varepsilon_{j+\frac{1}{2}} \left| \frac{u_{j+1} - u_j}{h} \right|^2$$

By $|u_{j+1} - u_j|^2 \leq 2 \left(|u_{j+1}|^2 + |u_j|^2 \right)$, we deduce,

$$\int_{\mathbb{R}} \mu(\cdot, \mathbf{x}_T)^{-1} |u_h'|^2 \leq \frac{4\, c_+^2}{h^2} \sum_{j \in Z} \varepsilon_{j+\frac{1}{2}} \left(\frac{|u_j|^2 + |u_{j+1}|^2}{2} \right) h = \frac{4\, c_+^2}{h^2} \oint_{\mathbb{R}} \varepsilon(\cdot, \mathbf{x}_T)\, |u_h|^2,$$

by definition of the 1D quadrature formula (26). ■

3 Application to the validation of a simplified 1D model

3.1 Recap about the "1D" limit model

The asymptotic analysis of thin co-axial cables with respect to the small thickness of the cable has been led in [16, 17] (see also [4, 6, 7] for extensions and more elaborated models). What follows is mainly extracted from [16]. Roughly speaking the 1D model is obtained from a rigorous asymptotic analysis of a family of domains parametrized by a strictly positive scalar $\delta > 0$ and that are defined as the result of a *transverse scaling* of a reference cable Ω. More precisely we introduce

$$\Omega^\delta = \mathcal{G}_\delta \big(\Omega \big),$$

where $\mathcal{G}_\delta$ is the transformation $\mathcal{G}_\delta : (x_1, x_2, x_3) \longrightarrow (\delta x_1, \delta x_2, x_3)$. Accordingly, for each $\delta > 0$, we consider $(\varepsilon^\delta, \mu^\delta, \sigma^\delta)$, defined in Ω^δ, respectively the permittivity, permeability and conductivity of the cable Ω^δ obtained from the ones for the reference cable Ω by a simple mapping, namely,

$$\varepsilon^\delta = \varepsilon \circ \mathcal{G}_\delta^{-1}, \quad \mu^\delta = \mu \circ \mathcal{G}_\delta^{-1}, \quad \sigma^\delta = \sigma \circ \mathcal{G}_\delta^{-1},$$

and we consider the family of problems, with unknown $\mathbf{E}^\delta(\mathbf{x}, t) : \Omega^\delta \times \mathbb{R}^+ \to \mathbb{R}^3$,

$$\left\{ \begin{array}{ll} \varepsilon^\delta\, \partial_t \mathbf{E}^\delta + \sigma^\delta\, \mathbf{E}^\delta - \boldsymbol{\nabla} \times \mathbf{H}^\delta = \mathbf{0}, & \text{in } \Omega^\delta \times \mathbb{R}^+. \\ \mu^\delta\, \partial_t \mathbf{H}^\delta + \boldsymbol{\nabla} \times \mathbf{E}^\delta = \mathbf{0}, & \text{in } \Omega^\delta \times \mathbb{R}^+, \\ \mathbf{E}^\delta \times \mathbf{n} = 0, & \text{on } \partial\Omega^\delta \times \mathbb{R}^+, \end{array} \right. \tag{60}$$

completed with the initial conditions

$$\mathbf{E}^\delta(\cdot, 0) = \mathbf{E}_0^\delta, \quad \mathbf{H}^\delta(\cdot, 0) = \mathbf{H}_0^\delta, \quad \mathbf{E}_0^\delta := \mathbf{E}_0 \circ \mathcal{G}_\delta^{-1}, \quad \mathbf{H}_0^\delta := \mathbf{H}_0 \circ \mathcal{G}_\delta^{-1}. \tag{61}$$

In order to state our asymptotic result, we first rescale the fields in the fixed domain Ω setting

$$\widetilde{\mathbf{E}}^\delta(\mathbf{x}, \mathbf{t}) := \mathbf{E}^\delta(\mathcal{G}_\delta \mathbf{x}, \mathbf{t}), \quad \widetilde{\mathbf{H}}^\delta(\mathbf{x}, \mathbf{t}) := \mathbf{H}^\delta(\mathcal{G}_\delta \mathbf{x}, \mathbf{t}), \quad \forall\, \mathbf{x} \in \boldsymbol{\Omega}, \tag{62}$$

and it is useful to introduce a cut Σ of the cross S, namely a line $\Gamma \subset \overline{\Omega}$ that joins the interior boundary Γ_i to the exterior boundary Γ_e in such a way that the open set $\Omega \setminus \Gamma$ is simply connected. We then define accordingly,

$$H^1_\Sigma(S) = H^1(S \setminus \Sigma) \quad \text{ and } \quad \widetilde{H}^1_\Sigma(\Omega) := \big\{ u \in H^1_\Sigma(S) \;/\; \int_S u\, d\mathbf{x}_T = 0 \big\}. \tag{63}$$

In what follows, $\big[u\big]_\Sigma$ denotes the jump of u across Σ (properly defined in [16], Section 3.1). Then, one can show (see for instance ([17], [4] and [26] in a more general context) that, if the initial data are well-prepared, (cf. (71) and remark 3.1)

$$\begin{aligned} \widetilde{\mathbf{E}}^\delta(\mathbf{x},t) &\underset{\delta\to 0}{\sim} \widetilde{\mathbf{E}}^0(\mathbf{x},t) := V(x_3,t)\,\nabla_T\varphi(\mathbf{x}_T,x_3) + \int_0^t V(x_3,t-s)\,\nabla_T\varphi_r(\mathbf{x}_T,x_3,s)\,ds, \\ \widetilde{\mathbf{H}}^\delta(\mathbf{x},t) &\underset{\delta\to 0}{\sim} \widetilde{\mathbf{H}}^0(\mathbf{x},t) := I(x_3,t)\,\nabla_T\psi(\mathbf{x}_T,x_3), \end{aligned} \tag{64}$$

where, in the formulae (64),

(i) the potentials $\varphi(\cdot,x_3)\in H^1_0(S)$ and $\psi(\cdot,x_3)\in \widetilde{H}^1_\Sigma(S)$ are defined, for each x_3 that plays the role of a parameter, as the solutions of the following boundary value problems (see the comments below for more details and subtleties concerning ψ),

$$\left\{\begin{array}{ll} \mathrm{div}_T\big(\varepsilon(\cdot,x_3)\,\nabla_T\varphi(\cdot,x_3)\big)=0 & \text{in } \Omega, \\ \varphi(\cdot,x_3)=1 & \text{on } \Gamma_i, \\ \varphi(\cdot,x_3)=0 & \text{on } \Gamma_e, \end{array}\right. \qquad \left\{\begin{array}{ll} \mathrm{div}_T\big(\mu(\cdot,x_3)\,\nabla_T\psi(\cdot,x_3)\big)=0 & \text{in } \Omega\setminus\Sigma, \\ \partial_n\psi(\cdot,x_3)=0 & \text{on } \partial S, \\ \big[\psi(\cdot,x_3)\big]_\Sigma=1,\ \big[\partial_n\psi(\cdot,x_3)\big]_\Sigma=0 & \text{across } \Sigma, \end{array}\right. \tag{65}$$

(ii) the functions $\varphi_r(\cdot,x_3,\cdot): S\times\mathbb{R}^+$ is defined, for each x_3, by the formulae,

$$\varphi_r(\cdot,x_3,t)=e^{-t\,\mathbf{A}(x_3)}\,\varphi_{r,0}(\cdot,x_3)\in C^\infty\big(\mathbb{R}^+,H^1_0(S)\big), \tag{66}$$

where $\mathbf{A}(x_3)\in\mathcal{L}\big(H^1_0(S)\big)$ is the bounded positive definite symmetric operator defined by

$$u:=\mathbf{A}(x_3)\,v \iff u\in H^1_0(S) \text{ and } \mathrm{div}_T\big(\varepsilon(\cdot,x_3)\nabla_T u\big) = \mathrm{div}_T\big(\sigma(\cdot,x_3)\nabla_T v) \text{ in } S. \tag{67}$$

and where $\varphi_{r,0}(\cdot,x_3):=-\mathbf{A}(x_3)\varphi\in H^1_0(S)$.

(iii) The voltage $V(x_3,t)$ and the current $I(x_3,t)$ are solution of the generalized telegrapher's equation (this is the 1D limit model)

$$\left\{\begin{array}{l} C(x_3)\,\partial_t V(x_3,t)+G(x_3)\,V(x_3,t)+\partial_3 I(x_3,t)+\displaystyle\int_0^t k(x_3,t-s)\,V(x_3,s)\,ds=0, \\ L(x_3)\,\partial_t I(x_3,t)+\partial_3 V(x_3,t)=0, \end{array}\right. \tag{68}$$

where the effective coefficients $C(x_3)>0, G(x_3)\geq 0$ and $L(x_3)>0$ are given by

$$\left\{\begin{array}{l} C(x_3)=\displaystyle\int_S \varepsilon(\mathbf{x}_T,x_3)\,|\nabla_T\varphi(\mathbf{x}_T,x_3)|^2\,d\mathbf{x}_T, \\ G(x_3)=\displaystyle\int_S \sigma(\mathbf{x}_T,x_3)\,|\nabla_T\varphi(\mathbf{x}_T,x_3)|^2\,d\mathbf{x}_T, \\ L(x_3)=\displaystyle\int_S \mu(\mathbf{x}_T,x_3)\,|\nabla_T\psi(\mathbf{x}_T,x_3)|^2\,d\mathbf{x}_T, \end{array}\right. \tag{69}$$

and the kernel $k(x,t)$ is given by

$$k(x_3,t)=\int_{S_{x_3}}\sigma(\mathbf{x}_T,x_3)\,\nabla_T\varphi_r(\mathbf{x}_T,x_3,t)\cdot\nabla_T\varphi(\mathbf{x}_T,x_3). \tag{70}$$

By well-prepared data we meant that,

$$\left\{\begin{array}{l} \mathbf{E}^\delta_0(\mathbf{x}_T,x_3)=V_0(x_3)\nabla_T\varphi(\mathbf{x}_T,x_3)+O(\delta) \\ \mathbf{H}^\delta_0(\mathbf{x}_T,x_3)=I_0(x_3)\nabla_T\psi(\mathbf{x}_T,x_3)+O(\delta), \end{array}\right. \tag{71}$$

and complete the generalized telegrapher's equation (68) with the initial conditions

$$V(x_3,0)=V_0(x_3) \quad \text{and} \quad I(x_3,0)=I_0(x_3). \tag{72}$$

Remark 3.1 (Well prepared data)**.** *The reconstruction formulae given in* (64) *correspond to well prepared initial conditions* (71)*. It is also possible to consider general initial data, i-e*

$$\begin{cases} \mathbf{E}_0^\delta(\mathbf{x}_T,x_3)=V_0(x_3)\nabla_T\varphi(\mathbf{x}_T,x_3)+\mathbf{E}_{0,T}^r+O(\delta), \\ \mathbf{H}_0^\delta(\mathbf{x}_T,x_3)=I_0(x_3)\nabla_T\psi(\mathbf{x}_T,x_3)+\mathbf{H}_{0,T}^r+O(\delta), \end{cases} \tag{73}$$

where $\left(\mathbf{E}_{0,T}^r,\,\mathbf{H}_{0,T}^r\right)$ *are purely transverse fields that must satisfy for each* x_3*,*

$$\begin{cases} rot_T\mathbf{E}_{0,T}^r(\cdot,x_3)=0 & \text{in } \Omega, \\ \mathbf{E}_{0,T}^r(\cdot,x_3)\times n_T=0, & \text{on } \partial\Omega, \end{cases} \qquad \begin{cases} rot_T\mathbf{H}_{0,T}^r(\cdot,x_3)=0 & \text{in } \Omega, \\ \mathbf{h}_{0,T}^r(\cdot,x_3)\cdot n_T=0, & \text{on } \partial\Omega, \end{cases} \tag{74}$$

In that case, the asymptotic formula (64) *is still valid up to the addition of quasi-static field that is not propagating. In particular, if the initial data have a compact support, these quasi-static fields vanish outside this support which means that* (64) *is still valid outside this support.*

The above asymptotic results and formulas deserve the following comments:

(a) In all above formulas, $\psi(\cdot,x_3)$ being discontinuous across Σ, $\nabla_T\psi(\cdot,x_3)\in L^2(S)^2$ has to be understood in the sense of $\mathcal{D}'(S_\Sigma)$. Let us emphasize that, if $\psi(\cdot,x_3)$ depends of course on the choice of the Σ, $\nabla_T\psi(\cdot,x_3)$ does not ! (see for instance [16], formula (33)).

(b) In the limit $\delta\to 0$, (64) shows that the longitudinal fields E_3^δ and H_3^δ vanish. In other words the limit fields are transversely polarized. Moreover, the formulae point out the existence of a kind of asymptotic separation of variables between longitudinal and transverse variable. In particular, the time dependence of the limit fields is entirely contained in the 1D (in space) functions $V(x_3,t)$ and $I(x_3,t)$.

(c) It is remarkable that the presence of the conductivity σ induces the apparition of non local effects in time through the presence of the time convolution term appearing in the first equation of (68). On the other hand, when $\sigma=0$, (68) is nothing but a 1D wave equation with variable coefficients.

(d) The well posedness and stability of the evolution are ensured by the following positivity property (see Lemma 5.2 in [16]), valid for any $T\geq 0$ and any $\xi\in L^2_{loc}(\mathbb{R}^+)$

$$G(x_3)\int_0^T |\,\xi(t)\,|^2\,dt\;+\int_0^T\int_0^t k(x_3,t-s)\,\xi(s)\,\xi(t)\,ds\,dt\;\geq 0. \tag{75}$$

(e) We notice that from the definition (64) of the limit field $\widetilde{\mathbf{E}}^0(\mathbf{x},t)\equiv\widetilde{\mathbf{E}}_T^0(\mathbf{x},t)$, one has

$$V(x_3,t)=C(x_3)^{-1}\int_S \varepsilon(\cdot,x_3)\,\widetilde{\mathbf{E}}_T^0(\cdot,x_3,t)\cdot\nabla_T\varphi(\cdot,x_3)\,d\mathbf{x}_T$$

because it follows from the definition (74) of φ and form the fact the $\varphi_r(\cdot,t)\in H_0^1(S)$ that

$$\forall\, t>0,\quad \int_S \varepsilon(\cdot,x_3)\,\nabla_T\varphi_r(\cdot,x_3,t)\cdot\nabla_T\varphi(\cdot,x_3)\,d\mathbf{x}_T=0.$$

This suggests to define a 1D voltage $V^\delta(x_3,t)$ for the 3D problem as

$$V^\delta(x_3,t)=C(x_3)^{-1}\int_S \varepsilon(\cdot,x_3)\,\widetilde{\mathbf{E}}_T^\delta(\cdot,x_3,t)\cdot\nabla_T\varphi(\cdot,x_3)\,d\mathbf{x}_T. \tag{76}$$

3.2 Numerical resolution of the telegrapher's equations

Even though this question is not the main purpose of the present paper, the main lines of the approach deserve to be explained. These consist in three phases:

(I) Precomputation of the coefficients of the model

It is a preliminary step that only consists in solving 2D problems in the cross section S:

- Numerical computation of the potentials (φ, ψ) and the coefficients $C(x_3), G(x_3)$ and $L(x_3)$.

  The potentials $(\varphi(\cdot, x_3), \psi(\cdot, x_3))$ are first approximated thanks to a $\mathbb{P}_1$ finite-elements approximation of the boundary value problems (74) with a triangular mesh of the cross section S with step-size h_T (this mesh "respects" the cut Σ), producing

  $$(\varphi_{h_T}(\cdot, x_3), \psi_{h_T}(\cdot, x_3)) \in V_{0,h_T} \times \widetilde{V}_{\Sigma,h_T},$$

  where V_{0,h_T} and $\widetilde{V}_{\Sigma,h_T}$ are the respective Galerkin approximation subspaces for $H^1_0(S) \times H^1_\Sigma(S)$ Then $C(x_3), L(x_3)$ and $L(x_3)$ are approximated, according to (69), by

  $$\left\{ \begin{aligned} C_{h_T}(x_3) &= \int_S \varepsilon(\mathbf{x}_T, x_3)\, |\nabla_T \varphi_{h_T}(\mathbf{x}_T, x_3)|^2 \, d\mathbf{x_T} \\ G_{h_T}(x_3) &= \int_S \sigma(\mathbf{x}_T, x_3)\, |\nabla_T \varphi_{h_T}(\mathbf{x}_T, x_3)|^2 \, d\mathbf{x_T} \\ L_{h_T}(x_3) &= \int_S \mu(\mathbf{x}_T, x_3)\, |\nabla_T \psi_{h_T}(\mathbf{x}_T, x_3)|^2 \, d\mathbf{x_T} \end{aligned} \right. \tag{77}$$

  Note that, from well known properties of conforming Galerkin methods one has

  $$C_{h_T}(x_3) \geq C(x_3), \quad G_{h_T}(x_3) \geq G(x_3), \quad L_{h_T}(x_3) \geq L(x_3) \tag{78}$$

- Numerical approximation of the function φ_r and kernel $k(x_3, t)$.

  One first realizes a finite dimensional approximation of the operator $\mathbf{A}(x_3)$ via a $\mathbb{P}_1$ finite-elements approximation (using the same mesh as above) of (67). This produces

  $$\mathbf{A}_{h_T}(x_3) \in \mathcal{L}\big(V_{0,h_T}\big)$$

  that is easily proven to be uniformly bounded with respect to h_T. Then for each x_3, $\varphi_r(\cdot, x_3) \equiv \varphi_r(\mathbf{x}_T, x_3, t)$ is approximated by the solution $\varphi_r(\cdot, t, x_3)$ of the ordinary differential equation

  $$\frac{\mathrm{d}\varphi_{r,h_T}(\cdot, x_3)}{dt} + \mathbf{A}_{h_T}(x_3)\, \varphi_{r,h_T}(\cdot, x_3) = 0, \quad \varphi_{r,h_T}(\cdot, x_3, 0) = -\mathbf{A}_{h_T}(x_3)\varphi_{h_T}(\cdot, x_3).$$

  that is consistent with the expression (66). The above differential system is not stiff and can thus be efficiently solved numerically with any ODE solver (Euler, Crank-Nicolson, Runge-Kutta, ...). Finally, the convolution kernel $k(x_3)$ is approximated, consistently with (70), by

  $$k_{h_T}(x_3, t) := \int_S \sigma(\mathbf{x}_T, x_3)\, \nabla_T \varphi_{r,h_T}(\mathbf{x}_T, x_3, t) \cdot \nabla_T \varphi_{h_T}(\mathbf{x}_T, x_3)\, d\mathbf{x}_T. \tag{79}$$

(II) Resolution of the 1D evolution problem

The semi-discretization in space of does not pose any particular problem : it can be done, for instance, using 1D mixed finite elements (for instance continuous $\mathbb{P}_1$ for V (cf. (50)) and discontinuous $\mathbb{P}_0$ for I) and mass lumping with a uniform mesh of step-size h. The resulting algebraic problem takes the form

$$\left\{\begin{aligned} &\mathbf{M}_{\mathrm{e},\mathbf{h}}\,\frac{\mathrm{d}\mathbb{V}_{\mathbf{h}}}{\mathrm{d}t}+\mathbf{M}_{\mathrm{c},\mathbf{h}}\,\mathbb{V}_h+\mathbf{D}_{\mathbf{h}}\,\mathbb{I}_h+\int_0^t\mathbf{K}_{\mathbf{h}}(t-s)\,\mathbb{V}_h(s)\,ds=0,\\ &\mathbf{M}_{\mathrm{m},\mathbf{h}}\,\frac{\mathrm{d}\,\mathbb{I}_{\mathbf{h}}}{\mathrm{d}t}-\mathbf{D}^*_{\mathbf{h}}\,\mathbb{V}_h=0,\end{aligned}\right. \tag{80}$$

where $\mathbb{V}_{\mathbf{h}}(t)=\big(V_j(t)\big)$ is the vector of degrees of freedom at time t for the semi-discrete voltage $V_{\mathbf{h}}(t)\in H^1(\mathbb{R})$ (the nodal values at the points jh), $\mathbb{I}_{\mathbf{h}}(t)=\big(I_{j+\frac12}(t)\big)$ the vector of degrees of freedom at time t for the current $I_{\mathbf{h}}(t)\in H^1(\mathbb{R})$ (namely the mean values in the intervals $[jh,(j+1)h]$) and

- $\mathbf{M}_{\mathrm{e},\mathbf{h}}=\mathrm{diag}\big(m_{\mathrm{e},j}\big)>0$, $\mathbf{M}_{\mathrm{c},\mathbf{h}}=\mathrm{diag}\big(m_{\mathrm{c},j}\big)\geq 0$ and $\mathbf{M}_{\mathrm{m},\mathbf{h}}=\mathrm{diag}\big(m_{\mathrm{m},j+\frac12}\big)>0$ are diagonal mass (like) matrices (divided by h for homogeneity) with
$$m_{\mathrm{e},j}=C_{h_T}(jh),\quad m_{\mathrm{c},j}=C_{h_T}(jh),\quad m_{\mathrm{m},j+\frac12}=C_{h_T}((j+\tfrac12)h)$$
- $\mathbf{K}_{\mathbf{h}}(t)=\mathrm{diag}\big(k_j(t)\big)$ is for each t a diagonal matrix with (see (79))
$$k_j(t):=\int_S\sigma(\mathbf{x}_T,jh)\,\nabla_T\varphi_{r,h_T}(\mathbf{x}_T,jh,t)\cdot\nabla_T\varphi_{h_T}(\mathbf{x}_T,jh)\,d\mathbf{x}_T.$$
- $\mathbf{D}_{\mathbf{h}}$ is a rectangular matrix that represents a discrete differentiation operator in x_3 for the current (as well as $-\mathbf{D}^*_{\mathbf{h}}$ for the voltage).

Concerning the time discretization it is natural to use a leap-frog (or Stormer-Verley) scheme with a constant time step and a staggered grid. The only non-standard part is the way one discretizes the convolution involving $\mathbf{K}_{\mathbf{h}}(t)$. With obvious notation, the resulting (purely explicit) scheme reads

$$\left\{\begin{aligned} &\mathbf{M}_{\mathrm{e},\mathbf{h}}\,\frac{\mathbb{V}^{n+1}_{\mathbf{h}}-\mathbb{V}^n_{\mathbf{h}}}{\Delta t}+\mathbf{M}_{\mathrm{c},\mathbf{h}}\,\frac{\mathbb{V}^{n+1}_{\mathbf{h}}+\mathbb{V}^n_{\mathbf{h}}}{2}+\mathbf{D}_{\mathbf{h}}\,\mathbb{I}^{n+\frac12}_h+\sum_{m=0}^{n}\mathbf{K}^{n-m}_{\mathbf{h}}\,\frac{\mathbb{V}^{m+1}_{\mathbf{h}}+\mathbb{V}^m_{\mathbf{h}}}{2}\,\Delta t=0,\\ &\mathbf{M}_{\mathrm{m},\mathbf{h}}\,\frac{\mathbb{I}^{n+\frac12}_{\mathbf{h}}-\mathbb{I}^{n-\frac12}_{\mathbf{h}}}{\Delta t}-\mathbf{D}^*_{\mathbf{h}}\,\mathbb{V}^n_h=0,\end{aligned}\right. \tag{81}$$

where the unknowns in the above system are

$$\left\{\begin{aligned} &\mathbb{V}^n_{\mathbf{h}}\quad\text{is the vector of degrees of freedom of } V^n_{\mathbf{h}}\in H^1(\mathbb{R}),\qquad\text{approximation of } V_{\mathbf{h}}(t^n),\\ &\mathbb{I}^{n+\frac12}_{\mathbf{h}}\ \text{is the vector of degrees of freedom of } I^{n+\frac12}_{\mathbf{h}}\in L^2(\mathbb{R}),\quad\text{approximation of } I_{\mathbf{h}}(t^{n+\frac12}),\end{aligned}\right.$$

and where the matrix $\mathbf{K}^p_{\mathbf{h}}$ is defined as follows

$$\mathbf{K}^p_{\mathbf{h}}=\mathrm{diag}\big(k^p_j\big),\quad k^p_j=\frac{1}{\Delta t^2}\int_0^{\Delta t}\int_0^{\Delta t}k_e(jh,r-s+p\Delta t)\,ds\,dr. \tag{82}$$

The theoretical interest of choosing $\mathbf{K}^p_{\mathbf{h}}$ as defined by (82) is clarified by the following lemmas which provides a discrete counter-part to the positivity property (75).

Lemma 3.2. *For any $j\in\mathbb{Z}$ and any real sequence $\xi^n, n\in\mathbb{N}$, one has the (discrete) positivity property*

$$G(jh)\sum_{n=0}^{N}|\xi^n|^2\,\Delta t\ +\sum_{n=0}^{N}\sum_{m=0}^{n}k^{n-m}_j\,\xi^n\,\xi^m\,\Delta t^2\ \geq 0. \tag{83}$$

Proof. Let w_j be the $\mathbb{P}_1$ hat function associated to the node jh, we introduce $\xi_j^{\Delta t}(t)$ defined by

$$\xi^{\Delta t}(t) = \frac{\xi^{m+1} + \xi^m}{2} \text{ for } t \in \left[t^m, t^{m+1}\right] \text{ and } 0 \leq m \leq n, \quad \xi^{\Delta t}(t) = 0 \text{ if } t > t_n.$$

Then, one can compute directly that

$$\left|\begin{aligned} & G(jh) \sum_{n=0}^{N} |\xi^n|^2 \, \Delta t \; + \sum_{n=0}^{N} \sum_{m=0}^{n} k_j^{n-m} \, \xi^n \, \xi^m \, \Delta t^2 = \\ & \qquad G(jh) \int_0^T |\, \xi^{\Delta t}(t) \,|^2 \, dt \; + \int_0^T \int_0^t k(jh, t-s) \, \xi^{\Delta t}(s) \, \xi^{\Delta t}(t) \, ds \, dt \; \geq 0 \end{aligned}\right.$$

and one concludes with (75). ■

Using Lemma 3.2 and standard energy techniques, it is easy to prove the stability result below.

Theorem 3.3. The numerical scheme (81) is L^2-stable under the sufficient CFL condition

$$c_{h_T}^+ \, \frac{\Delta t}{h} \leq 1, \quad c_{h_T}^+ = \sup_{x_3 \in \mathbb{R}} c_{h_T}(x_3), \quad c_{h_T}(x_3) := C_{h_T}(x_3)^{-\frac{1}{2}} L_{h_T}(x_3)^{-\frac{1}{2}}, \tag{84}$$

where the function $c_{h_T}(x_3)$ satisfies the uniform (in x_3) convergence property (see also (78))

$$c_{h_T}(x_3) \leq c_{1D}(x_3), \quad \lim_{h_T \to 0} c_{h_T}(x_3) = c_{1D}(x_3), \quad c_{1D}(x_3) := C(x_3)^{-\frac{1}{2}} L(x_3)^{-\frac{1}{2}}.$$

Remark 3.4 (Comparison with the 3D stability condition)**.** *According to Theorem 3.3, an asymptotically optimal (when $h_T \to 0$) sufficient CFL condition is*

$$c_{1D}^+ \, \frac{\Delta t}{h} \leq 1, \quad c_{1D}^+ := \sup_{x_3 \in \mathbb{R}} c_{1D}(x_3). \tag{85}$$

In order to compare with the CFL condition (53) *for the 3D problem, we need to compare c_{1D}^+ with c^+. However, it is shown in [16] that*

$$\forall \, x_3 \in \mathbb{R}, \quad c_{1D}(x_3) \leq \sup_{\mathbf{x}_T \in S} c(\mathbf{x}_T, x_3) \quad \textit{which implies } c_{1D}^+ < c^+$$

This shows that the 3D CFL condition (53) *is more restrictive than the 1D condition* (85)*. Indeed, if* (53) *holds,*

$$c_{1D}^+ \, \frac{\Delta t}{h} \leq c_+ \, \frac{\Delta t}{h} \leq \sqrt{\frac{4\theta - 1}{4\theta}} < 1.$$

(III) Reconstruction of the 3D electric field

Once the discrete voltage $V_h^n(x_3)$ is computed, according to (64), one can reconstruct the (rescaled) 3D electric field at time as the $\mathbb{P}_1$-interpolant of the following transverse fields, defined for each j, using a discrete convolution formula consistent with the one appearing in (81), namely,

$$\widetilde{\mathbf{E}}_j^n(\mathbf{x}_T, jh) = V_h^n(jh) \, \nabla \varphi(\mathbf{x}_T, jh) + \sum_{m=0}^{n-1} \frac{V^{m+1}(jh) + V^m(jh)}{2} \, \nabla_T \varphi_r(\mathbf{x}_T, jh, t^n - t^m) \, \Delta t. \tag{86}$$

4 Numerical experiments

In this section, we present numerical results aiming at illustrating, and even more quantifying, the asymptotic analysis presented Section 3.1. This will be done by solving the problem (60) for several values of δ using the numerical method presented Section 2, thus with the second order formulation (see (8) or equivalently (11)). Even more, to allow for a comparison between values of δ, we shall compute the rescaled field (cf. (62)) that have the advantage to be define in the reference geometry, as well as the asymptotic electric field appearing in (64). The only difference with respect to (11) is the apparition of δ-dependent terms in the equations through the simple substitution

$$\mathrm{rot}_T \to \delta^{-1}\,\mathrm{rot}_T, \quad \mathbf{rot}_T \to \delta^{-1}\,\mathbf{rot}_T, \quad \mathrm{div}_T \to \delta^{-1}\,\mathrm{div}_T, \quad \nabla_T \to \delta^{-1}\,\nabla_T,$$

which has no incidence on the numerical method of Section 2.

4.1 The data of the problem

We have chosen to treat a cable whose geometry has no circular symmetry. This geometry is represented Figure 8. The diameter of S is 4 and its intersection with the half-plane $x_1 > 0$ "coincides" with a circular annulus. More precisely:

$$S \cap \{x_1 > 0\} \equiv \{(x_1, x_2) \;/\; x_1 > 0 \text{ and } 1 \leq (x_1^2 + x_2^2)^{\frac{1}{2}} \leq 2\} \tag{87}$$

As the cut for the computation of the potential ψ (cf. (74)), we shall take the segment

$$\Sigma = [1, 2] \times \{0\}. \tag{88}$$

The numerical computations are done in the portion of cable $0 \leq x_3 \leq 10$. For simplicity, periodic boundary conditions will be applied between $x_3 = 0$ and $x_3 = 10$.

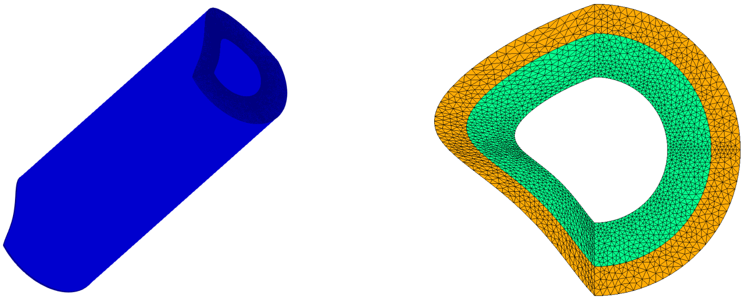

Fig. 8: Left: the domain Ω, Right: the section S of the domain. Each color correspond to a different material.

Concerning the coefficients of the model, we shall treat two cases

- The *unperturbed* case. This corresponds to the case where the coefficients of the model are invariant by translation in the longitudinal direction,

$$\varepsilon(\mathbf{x}_T, x_3) = \varepsilon^0(\mathbf{x}_T), \quad \mu(\mathbf{x}_T, x_3) = \mu^0(\mathbf{x}_T), \quad \sigma(\mathbf{x}_T, x_3) = \sigma^0(\mathbf{x}_T). \tag{89}$$

The cable is however heterogeneous is the cross sections S. More precisely S is made of two layers $S = S_1 \cup S_2$ and inside S_j, the material is homogeneous (see Figure 8),

$$\big(\varepsilon^0(\mathbf{x}_T), \mu^0(\mathbf{x}_T), \sigma^0(\mathbf{x}_T)\big) = (\varepsilon_j, \mu_j, \sigma_j) \quad \text{in } S_j. \tag{90}$$

In our numerical experiments we shall take $(\varepsilon_1, \mu_1) = (2, 2)$ and $(\varepsilon_2, \mu_2) = (1, 1)$ so that the velocity of electromagnetic waves, $c(\mathbf{x}) = (\varepsilon\mu)(\mathbf{x})^{-\frac{1}{2}}$ is

$$c(\mathbf{x}) = c_1 = 1/2 \text{ in } \Omega_1 := S_1 \times \mathbb{R}, \quad c(\mathbf{x}) = c_2 = 1 \text{ in } \Omega_2 := S_2 \times \mathbb{R}. \tag{91}$$

Concerning the conductivity, we shall consider two scenarios :

  - without any conductivity (*non conductive case.*) : $\sigma_1 = \sigma_2 = 0$,
  - with conductivity in Ω_2 (*conductive case.*) : $\sigma_1 = 0$, $\sigma_2 = 0.5$.
- The *perturbed* case. In this case, the translational invariance is broken because the coefficients may vary locally in x_3 near $x_3 = 6$. This can be reinterpreted as a localized damage of the cable. We take,

$$\varepsilon(\mathbf{x}_T, x_3) = \varepsilon^0(\mathbf{x}_T)\,\big(1 + p(x_3)\big), \quad \text{and the same for } \mu(\mathbf{x}_T, x_3) \text{ and } \sigma(\mathbf{x}_T, x_3). \tag{92}$$

  where p is a very localized Gaussian, supported in practice in $[5.75, 6.25]$ (see Figure 9),

$$p(x_3) := \pi\, e^{-80\, ln(2)(x_3-6)^2}. \tag{93}$$

We also take initial conditions which are localized near $x_3 = 5$ and are *well prepared* with respect to the expected asymptotic result (64). More precisely $\mathbf{H}_0(\mathbf{x}_T, x_3) = 0$ and

$$\mathbf{E}_0(\mathbf{x}_T, x_3) := \mathcal{E}(x_3)\ \nabla_T \varphi(\mathbf{x}_T, x_3), \quad \mathcal{E}(x_3) = e^{-\pi^2\,(x_3-5)^2} \tag{94}$$

In practice, the initial data are supported in $[4, 6]$ and will generate longitudinal with a wavelength $\lambda \simeq 1$.

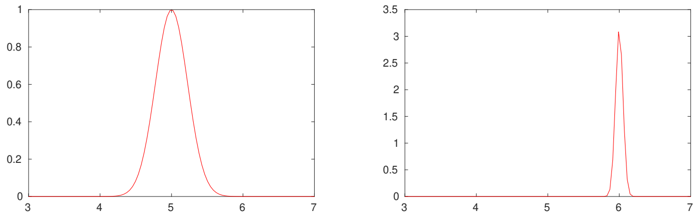

Fig. 9: The functions $\mathcal{E}(x_3)$ (left) and $p(x_3)$ (right).

The time interval for the numerical experiments will be $[0, T]$ with $T = 4$ so that, taking into account (91), implies that the waves will not reach the transverse boundaries $x_3 = 0$ and $x_3 = 10$ before the final time T: in other words, the periodic boundary conditions in x_3 will not play any role.

Note that the initial field is transversely polarized. However, due to the heterogeneity of the cable, it will not remain transversely polarized during the time (even in the unperturbed case, separation of variable does not work for Maxwell's equations) as the numerical results will illustrate it. Note also that, because of (74), $\mathbf{div}(\varepsilon\,\mathbf{E}_0) = 0$.

4.2 Discretization parameters

Data for the transverse discretization. The mesh of the cross section will be a triangular mesh represented Figure 8. In particular, there are 20 mesh points along the cut Σ and the typical diameter of each triangle in the mesh is

$$h_T \simeq 0.05.$$

This mesh is used for the $2D$ transverse problems (74,66,67) for computing the potentials $(\varphi, \psi, \varphi_r)$ and the coefficients (C, G, L) but also for the 3D computations. Because of the specific form of the coefficients $(\varepsilon, \mu, \sigma)$ for the perturbed case, see (92), the potentials $(\varphi, \psi, \varphi_r)$ coincide with the x_3-independent potentials $(\varphi^0, \psi^0, \varphi_r^0)$ for the unperturbed,

$$\varphi(\cdot, x_3) = \varphi^0(\cdot), \quad \psi(\cdot, x_3) = \psi^0(\cdot), \quad \varphi_r(\cdot, x_3) = \varphi_r^0(\cdot, t).$$

Thus, only $(\varphi^0, \psi^0, \varphi_r^0)$ need to be computed numerically. Accordingly, with obvious notation,

$$C(x_3) = \big(1 + p(x_3)\big)\ C^0, \quad \text{(the same for } G(x_3), L(x_3), k(x_3, t)).$$

Data for the longitudinal discretization. The longitudinal step size h will be taken $h = 1/17$ which is well adapted to the discretization of the Gaussian $\mathcal{E}(x_3)$ (see again Figure 9).

This longitudinal mesh will be used for the discretization of the 1D problem (81) (cf. (68)) but also for the 3D computations.

Data for the time discretization. For facilitating the comparison between the 1D and 3D results, we shall use the same time step Δt for both 1D and 3D computations. According to Remark 3.4, the choice of Δt will be constrained by the 3D condition (53). For the 3D calculations, we shall take $\theta = 1/3$, in which case (53) gives: $c^+ \frac{\Delta t}{h} \leq \frac{1}{2}$. In practice we shall choose $\Delta t = 0.95 \ h/(2 \ c^+)$.

4.3 Numerical results

4.3.1 The potentials $(\varphi^0, \psi^0, \varphi_r^0)$

We present in Figure 10 the computed potentials φ and ψ. The right picture shows at the same time the level lines of φ (who are "parallel" to the boundaries) and the ones of ψ (which intersect the boundaries). This illustrates that $\big(\varphi(x_1, x_2), \psi(x_1, x_2)\big)$ generalizes polar coordinates inside S.

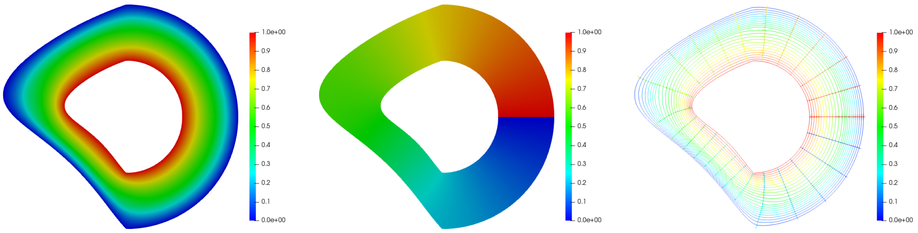

Fig. 10: Potentials φ (left) and ψ (center), associated isolines (right).

Figure 11 represents, via color levels, the evolution of $\varphi_r(t)$. We observe that $\varphi_r(t)$ tends to 0 when $t \to +\infty$, as expected from its definition (66) and the strict positivity of the operator $\mathbf{A}(x_3) \equiv \mathbf{A}$.

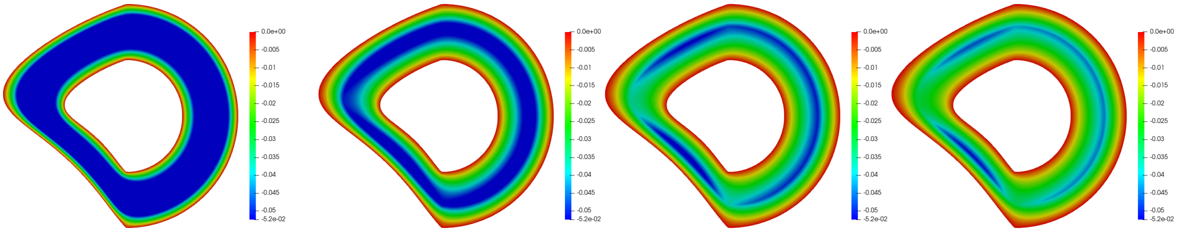

Fig. 11: Propagation of the $\varphi_r(t)$ field at $t_1 = 0$, $t_2 = 2.43$, $t_3 = 3.47$ and $t_4 = 4$.

Finally, we show Figure 12 the convolution kernel $k(t)$ that is negative (as proven in [16], Lemma 5.2) and tends also to 0 for large t.

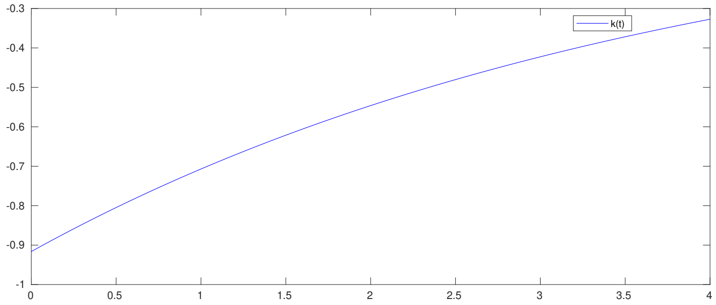

Fig. 12: The convolution kernel $k(t)$.

4.3.2 3D / 1D comparisons in the unperturbed case.

The non conductive case.

(a) Comparisons of voltages (in 1D). In figure 13, we compare the evolution of the 1D (limit) voltage $V(x_3, t)$ issued from the numerical resolution of the 1D limit model (68), to the 1D voltage $V^\delta(x_3, t)$ for the 3D problem, defined by (76) and obtained by post-processing the 3D solution $\widetilde{\mathbf{E}}_T^\delta$.

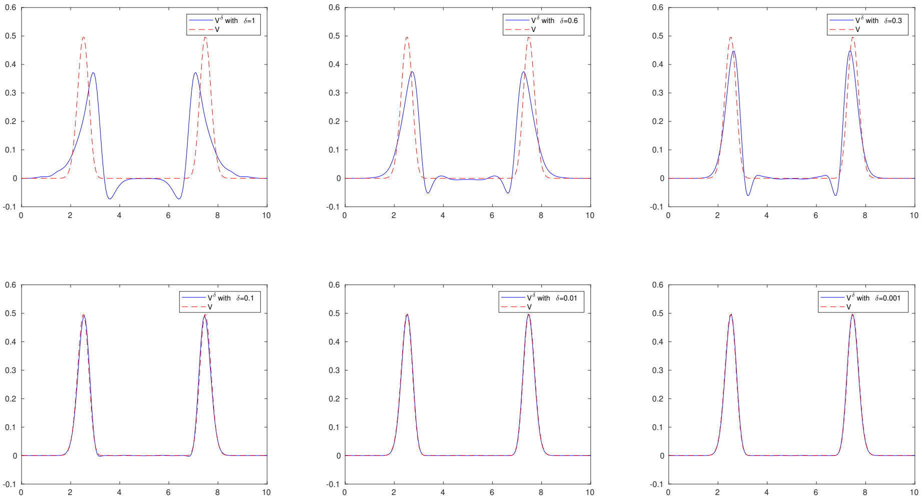

Fig. 13: The voltages V^δ and V at $t = 4$.

More precisely, we compare the above functions in space at the final time $T = 4$ for δ decreasing from 1 to 10^{-3}. The limit solution $V(x_3, T)$ is in red while $V^\delta(x_3, T)$ is in blue. The numerical results confirm the convergence of $V^\delta(x_3, t)$ towards $V(x_3, t)$. We observe that V and V^δ already almost coincide for $\delta = 0.1$. This corresponds to a cable diameter equal to 0.4, to be compared to the length of the support (in x_3) of the initial condition which is about 1 according to Figure 9.

(b) Comparison of the electric fields in 3D. We now compare, still at the final time $T = 4$, the norm of the electric field for $\delta > 0$ with its limit value. In figure 14, we represent $|\widetilde{\mathbf{E}}_T^\delta|$ on the boundary $\partial\Omega$ of the reference cable for $\delta = 1$ and $\delta = 10^{-3}$ and $\delta = 0$. We observe that the result obtained with $\delta = 10^{-3}$ can not be distinguished from the one obtained with the limit model while a substantial difference exists for

$\delta = 1$.

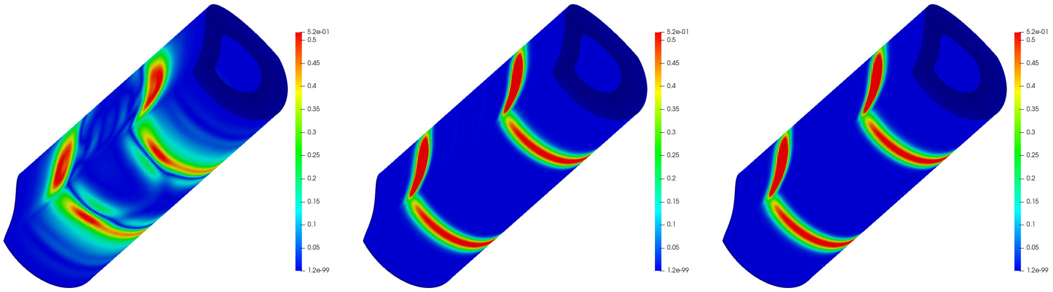

Fig. 14: Left $|\widetilde{\mathbf{E}}_T^\delta|$ with $\delta = 1$, Center $|\widetilde{\mathbf{E}}_T^\delta|$ with $\delta = 10^{-3}$, Right $|\widetilde{\mathbf{E}}_T^0|$ at $t = 4$.

In Figure 15, we make the same comparison in the cross section $x_3 = 2.71$ with roughly corresponds to the position of the wave at time $T = 4$ (see Figure 13). Again we observe that the results are very close for $\delta = 10^{-3}$ and $\delta = 0$, themselves quite different from the result obtained for $\delta = 1$.

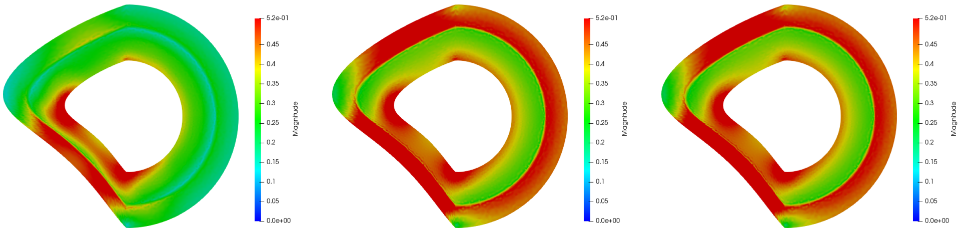

Fig. 15: Left $|\widetilde{\mathbf{E}}_T^\delta|$ with $\delta = 1$, Center $|\widetilde{\mathbf{E}}_T^\delta|$ with $\delta = 10^{-3}$, Right $|\widetilde{\mathbf{E}}_T^0|$ for $x_3 = 2.71$ and $t = 4$.

Finally, in order to test the asymptotic transverse polarization of the electric field, we represent Figure 16, again along $\partial\Omega$ at time $T = 4$ the longitudinal electric field $\widetilde{E}_3^\delta$. Let us draw the attention of the reader that the color scale is quite different from the ones in the figures 14 and 15. We observe that, as expected the longitudinal field tends to 0 when δ tends to 0. On the other hand, for $\delta = 1$ we see that, as announced previously, the field is really non transversely polarized even though the initial field is (cf. (94)): this confirms that separation of variables does not work.

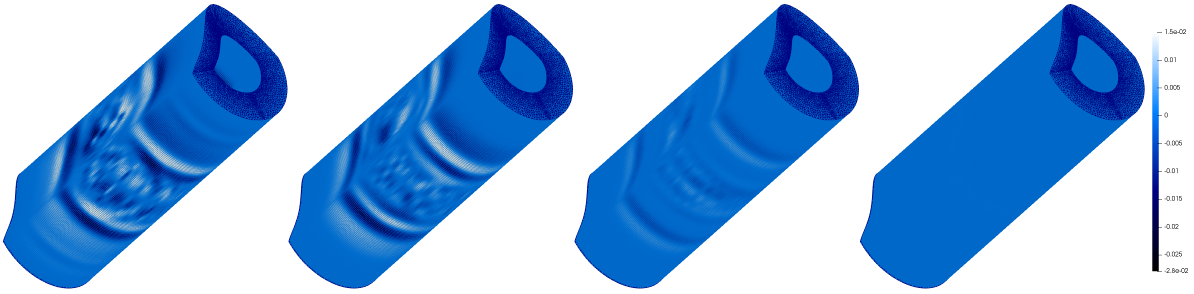

Fig. 16: E_3^δ with $\delta = 1$, $\delta = 0.5$, $\delta = 0.1$, $\delta = 0.001$ at $t = 4$.

The conductive case.

(a) Comparisons of voltages (in 1D). In figure 17, we compare the evolution of the 1D (limit) voltage $V(x_3, t)$ to the 1D voltage $V^\delta(x_3, t)$, exactly as in figure 13.

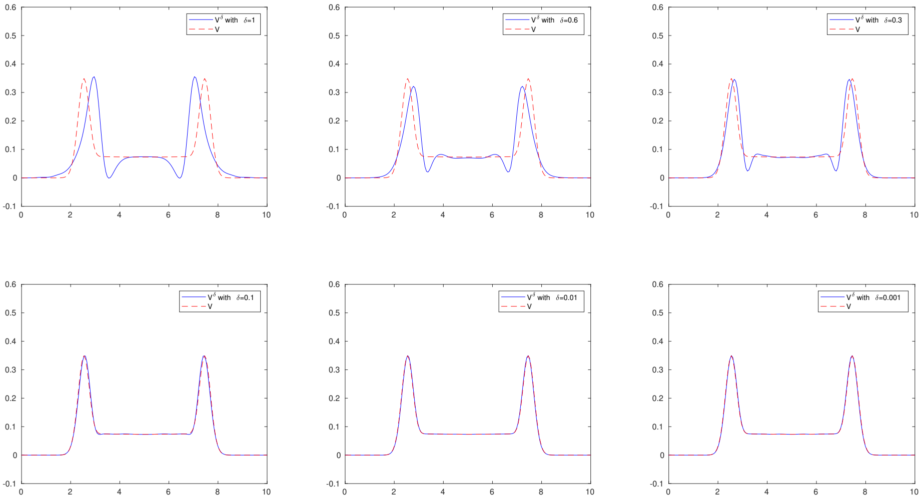

Fig. 17: The voltages V^δ and V at $t = 4$.

There are two main effects due to the conductivity (clearly visible on the limit blue curves) : the attenuation of the signal (compare the figures 13 and 17) and the shape of the wave. However, the convergence of $V^\delta(x_3, t)$ towards $V(x_3, t)$ is very similar to the one for the non conductive case for $\delta \leq 0.1$, but varying δ above 0.1 affects the waveform much more than in non conductive case.

(b) Comparison of the electric fields in 3D. We now compare in figure 18, still at the final time $T = 4$ on the boundary $\partial\Omega$, the norm of electric field for $\delta > 0$ with the one its limit value, exactly as in figure 14. The conclusions are the same than for the non conductive case.

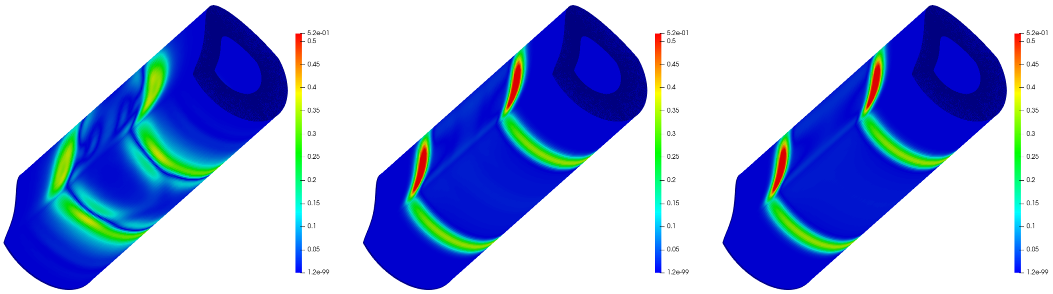

Fig. 18: Left $|\widetilde{\mathbf{E}}_T^\delta|$ with $\delta = 1$, Center $|\widetilde{\mathbf{E}}_T^\delta|$ with $\delta = 10^{-3}$, Right $|\widetilde{\mathbf{E}}_T^0|$ at $t = 4$.

4.3.3 The perturbed case.

The non conductive case.

(a) Comparisons of voltages (in 1D). As represented Figure 19, the main effect of the local perturbation is the apparition of reflection phenomena. We observe that the convergence to the limit solution is much slower than in the unperturbed case (compare with Figure 13): for instance, one needs $\delta = 0.01$ to get a correct localization of the reflected waves. This is probably due that we we have considered a strong defect with fast variations and large amplitude.

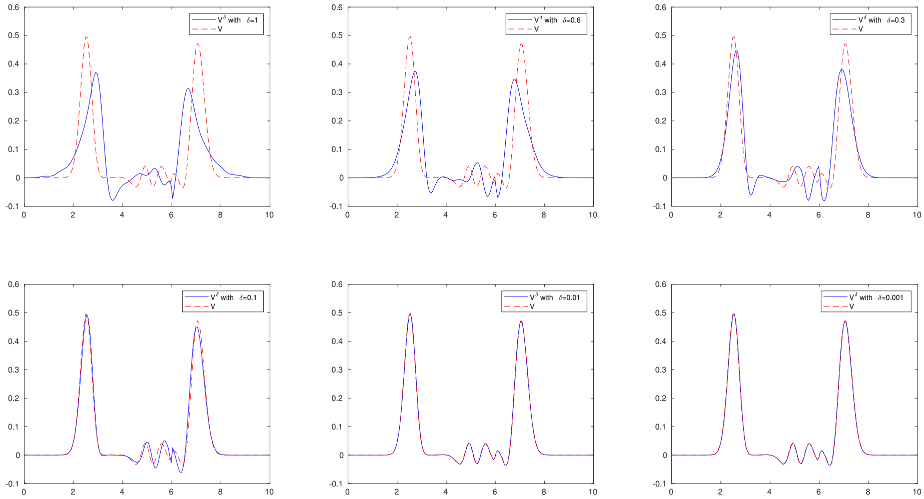

Fig. 19: The voltages V^δ and V at $t = 4$.

(b) Comparison of the electric fields in 3D. This is the object of Figure 20, to be compared with figure 14. In Figure 20, we represent the norm $|\widetilde{\mathbf{E}}^\delta_T|$ on the boundary $\partial\Omega$ of the reference cable for $\delta = 1$ and $\delta = 10^{-3}$ and $\delta = 0$. We observe that the norm of 3D field cannot be distinguished from the one of the limit field $\delta = 10^{-3}$ while a substantial difference exists for $\delta = 1$, and as found in the 1D results we also observe that the wave is reflected because of the perturbation localized at $x_3 = 6$.

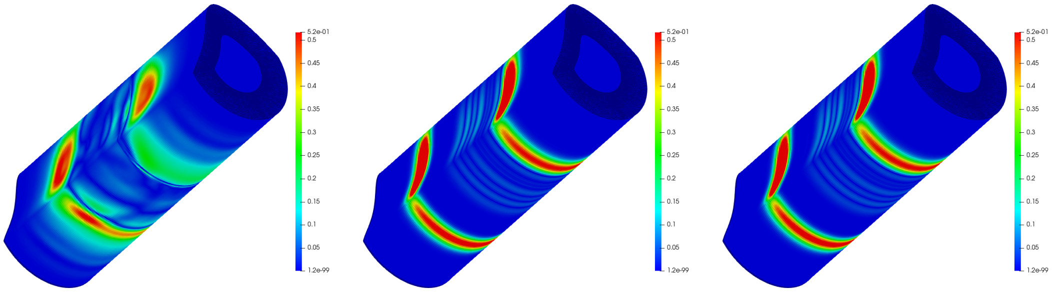

Fig. 20: Left $|\widetilde{\mathbf{E}}^\delta_T|$ with $\delta = 1$, Center $|\widetilde{\mathbf{E}}^\delta_T|$ with $\delta = 10^{-3}$, Right $|\widetilde{\mathbf{E}}^0_T|$ at $t = 4$.

The conductive case. We repeat in figures 21 and 22, the same experiments / comparisons than in figures 17 and 18 for the non conductive case, respectively for the 1D voltages and the 3D electric fields. Once again, one observes a big influence of the presence of the conductivity on the shape of the propagating wave. However, this does not affect the speed of convergence towards the limit model, which is quite similar to the one observed in the non conductive case.

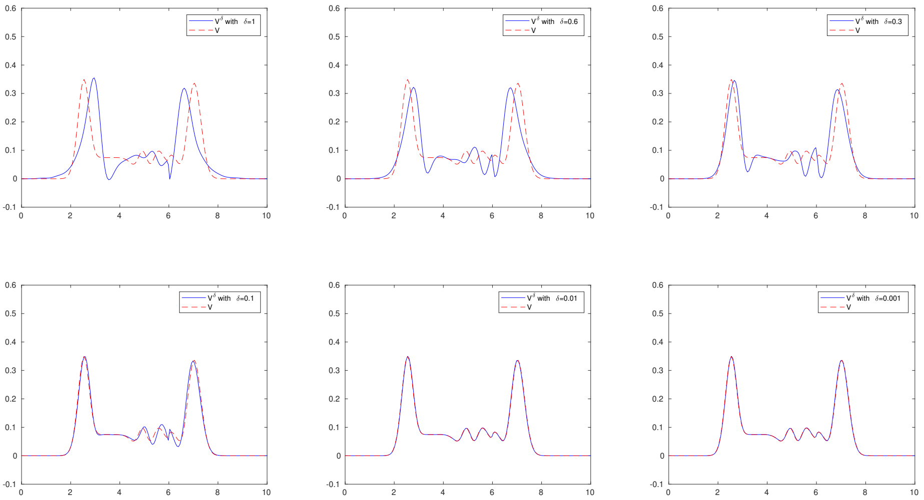

Fig. 21: The voltages V^δ and V at $t = 4$.

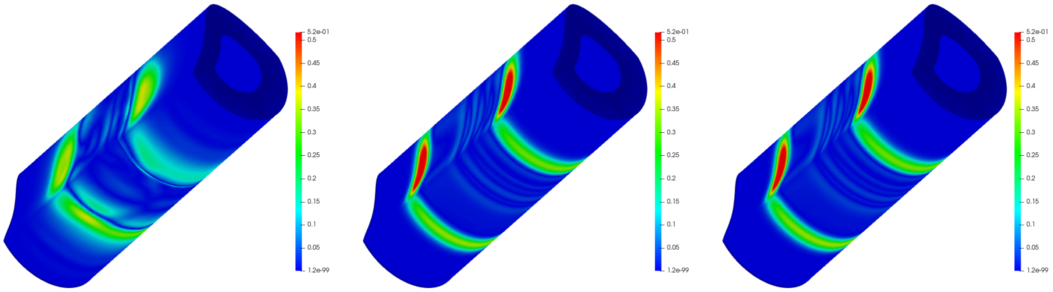

Fig. 22: Left $|\widetilde{\mathbf{E}}_T^\delta|$ with $\delta = 1$, Center $|\widetilde{\mathbf{E}}_T^\delta|$ with $\delta = 10^{-3}$, Right $|\widetilde{\mathbf{E}}_T^0|$ at $t = 4$.

5 Perspectives

We have presented an hybrid explicit-implicit time discretization combined with a space discretization of the Maxwell's equation based on edge's elements on prisms. The algorithm complexity of our method is low. The resulting scheme enabled to validate generalized 1D Telegrapher's equations. One important perspective of our work is to deal with non cylindrical geometry. This turns out to be a non-simple generalization that we aim to tackle with hybrid edge's element and the discontinuous Galerkin method. Although the question of convergence analysis (in space and time) of the proposed method is of interest and turn out not to be a straightforward application of known abstract results.

References

[1] M. Admane, M. Sorine, Q. Zhang. Inverse scattering for soft fault diagnosis in electric transmission lines, IEEE Trans. on Antennas and Propagation, Vol. 59, No. 1, 141–148, 2011.

[2] J. Albella Martínez, S. Imperiale, P. Joly and J. Rodríguez. Numerical analysis of a method for solving 2D linear isotropic elastodynamics with traction free boundary condition using potentials and finite elements. Mathematics of computations, Vol. 90, 1589–1636, 2021.

[3] F. Auzanneau. Wire troubleshooting and diagnosis: Review and perspectives. Progress In Electromagnetics Research B, Vol. 49, 253279, 2013.

[4] G. Beck. *Modélisation et étude mathématique de réseaux de câbles électriques. Modélisation et simulation,* Université Paris-Saclay, 2016.

[5] G. Beck. *Computer-implemented method for reconstructing the topology of a network of cables*, US patent n° : US20200363462A . 16/638,451, 2020. 2017, https://patents.google.com/patent/US20200363462A1/en.

[6] G.Beck, S. Imperiale and P. Joly. Mathematical modelling of multi conductor cables, Vol. 8, No. 3, 2014.

[7] G. Beck, S. Imperiale, P. Joly. *Asymptotic modeling of Skin-effects in coaxial cables*. Springer Nature: Part. Diff. Equ. and Applications, American Institute of Mathematical Science 1–42, 2020.

[8] M. Bergot, M. Duruflé. High-order optimal edge elements for pyramids, prisms and hexahedra, Journal of Computational Physics, Vol. 232, 189–213, 2013.

[9] A. Burel, S. Imperiale and P. Joly. Solving the homogeneous isotropic linear elastodynamics equations using potentials and finite elements. The case of the rigid boundary condition. Numerical Analysis and Applications, Vol. 5, No. 2, 136–143, 2012.

[10] J. Chabassier and S. Imperiale. Fourth-order energy-preserving locally implicit time discretization for linear wave equations, International journal for numerical methods in engineering, Vol. 106, No. 8, 593–622, 2015.

[11] J.-L. Coulomb, F.-X. Zgainski and Y. Marechal. A pyramidal element to link hexahedral, prismatic and tetrahedral edge finite elements, Institute of Electrical and Electronics Engineers, Vol. 33, No. 2, 1362–1365, 1997.

[12] S. Descombes, S. Lanteri and L. Moya. Locally Implicit Time Integration Strategies in a Discontinuous Galerkin Method for Maxwell's Equations, Vol. 56, No. 1, 190–218, 2012.

[13] M. Hochbruck and A. Sturm. Error Analysis of a Second-Order Locally Implicit Method for Linear Maxwell's Equations, SIAM Journal on Numerical Analysis, Vol. 54, No. 5, 3167–3191, 2016.

[14] M. Hochbruck and J. Leibold. an implicit-explicit time discretization scheme for second-order semilinear wave equations with application to dynamic boundary conditions, Vol. 147, No. 4, 869–899, 2021.

[15] M. Hochbruck, T. Jahnke and R. Schnaubelt. Convergence of an ADI splitting for Maxwell's equations, Numerische Mathematik, Vol. 129., No. 3, 535–561, 2014.

[16] S. Imperiale and P. Joly. Mathematical modeling of electromagnetic wave propagation in heterogeneous lossy coaxial cables with variable cross section, Applied Numerical Mathematics, Vol. 79, 42–61, 2014.

[17] S. Imperiale and P. Joly. Error estimates for 1D asymptotic models in coaxial cables with non-homogeneous cross-section. Advances in Applied Mathematics and Mechanics, Vol. 4, 647–664, 2012.

[18] A. Kameni, F.Loete, S.Ziani, K.Kahalerras, L. Pichon. Time domain modeling of soft faults in wiring system by a nodal Discontinuous Galerkin Method with high-order hexahedral meshes, proceeding of the IEEE International Conference on the Computation of Electromagnetic Fields, 2015.

[19] J. Lee and B. Fornberg. A split step approach for the 3-D Maxwell's equations. Journal of Computational and Applied Mathematics, Vol. 158, No. 2, 485–505, 2003.

[20] J. Lee and B. Fornberg. Some unconditionally stable time stepping methods for the 3D Maxwell's equations. Journal of Computational and Applied Mathematics, Vol. 166, No. 2, 497–523, 2004.

[21] J. Li, E.Machorro, S.Shields. Numerical study of signal propagation in corrugated coaxial cables, Journal of Computational and Applied Mathematics, Vol. 309, 230–243, 2017.

[22] P. Monk, Finite element methods for Maxwell's equations, Oxford science publications, 2003.

[23] J. C. Nedelec, Mixed finite elements in R3, Numer. Math. 35 (1980), 315–341.

[24] C. R. Paul. Analysis of Multiconductor Transmission Lines, Wiley-IEEE Press, 2008.

[25] T. Rylander, A. Bondeson. Stability of explicit-implicit hybrid time-stepping schemes for Maxwell's equations, Journal of Computational Physics, Vol. 179, No. 2, 426–438, 2002.

[26] S. Imperiale. Asymptotic analysis of abstract two-scale wave propagation problems, Working paper, hal-03306856, 2021.